Global Superstructure Optimisation of Red Blood Cell Production in a Parallelised Hollow Fibre Bioreactor

Ruth Misener[a,*], María Fuentes Garí[b], Maria Rende[b], Eirini Velliou[b], Nicki Panoskaltsis[c], Efstratios N. Pistikopoulos[b], Athanasios Mantalaris[b]

[a]*Department of Computing; Imperial College London; South Kensington SW7 2AZ; UK*
[b]*Department of Chemical Engineering; Imperial College London; South Kensington SW7 2AZ; UK*
[c]*Department of Haematology; Imperial College London; Northwick Park and St. Mark's Campus HA1 3UJ; UK*

Abstract

Recent work developed a novel, biomimetic, cost-effective three-dimensional hollow fibre bioreactor for growing healthy red blood cells *ex vivo* (Panoskaltsis et al., 2012). This bioreactor recapitulates architectural and functional properties of erythrocyte formation and thereby reduces the need for expensive growth factors by more than an order of magnitude. Individual experiments to empirically improve the bioreactor are intensive, so we propose global superstructure optimisation for bioreactor design. Our approach integrates topological design choices with operating conditions. Design choices include: number of parallelised bioreactors; number and type of hollow fibres; size and aspect ratio. Operating conditions are: feed concentrations; flowrate through the reactor. This manuscript quantitatively demonstrates, for the first time, the potential for *ex vivo* red blood cell production to compete openly against the transfusion market for rare blood. We discuss the potential of superstructure design not only on this individual bioreactor but also more generally on bioprocess optimisation.

Keywords: red blood cell production, bioreactor design, bioreactor operation, bioprocess optimisation, global superstructure optimisation

1. Introduction

Ninety-two million units of whole donor blood are globally collected yearly (World Health Organization, 2011). But despite the success of coordinated blood collection and utilisation: 3.3% of hospitals delay surgery because of blood shortages and 10.3% of hospitals experience at least one day yearly when blood needs cannot be met (Timmins and Nielsen, 2009; Whitaker and Henry, 2011). Beyond shortages of commonly-stocked blood types, patients undergoing regular transfusions may require expensive rare blood donation to mitigate the risk of an immune response to foreign antigens (Tahhan et al., 1994; Meny et al., 2013).

*r.misener@imperial.ac.uk; Tel: +44 (0) 20759 41361

Ex vivo blood production is an attractive solution for filling shortage gaps and scaling-up rare blood donations. But current blood expansion protocols require paying $8330 for nutrients and specialised proteins to produce one unit of red blood cells ($\approx 2 \times 10^{12}$ cells) when an average hospital in the USA pays only $225.42 for a typical unit of blood and $1150 to $3025 for a unit of rare blood (Timmins and Nielsen, 2009; Whitaker and Henry, 2011). Prices in the UK are similar: the National Health Service (NHS) spends an average of £125 per unit of red blood cells but up to £25k per patient episode for rare blood transfusions (Lawes, 2011).

Erythropoiesis, or red blood cell production, requires delivering nutrients, oxygen, and signalling proteins called growth factors to cells in a specialised 3D micro-environment known as the haematopoietic stem cell niche (Panoskaltsis et al., 2005). Although the 3D niche structure is crucial *in vivo*, typical *ex vivo* blood production methodologies are performed in 2D liquid suspension; these 2D *ex vivo* systems are expensive because they require artificially high levels of specialised growth factor proteins (Timmins and Nielsen, 2009). Beyond price, artificially high growth factor levels may introduce cell-altering artefacts into the *in vitro* culture (Ganser et al., 1988).

In this arena of erythrocyte production: recent work has developed a novel, biomimetic, cost effective 3D hollow fibre bioreactor for growing healthy blood *ex vivo* (Macedo, 2011; Panoskaltsis et al., 2012). This bioreactor is extremely promising because it reduces the need for growth factors by an order of magnitude by recapitulating the architectural and functional properties of blood formation. Although the blood-producing bioreactor yields red blood cells with correct: oxygen-carrying capacity, surface markers, and shape, individual experiments on the bioreactor are cost- and labour-intensive, so we propose deterministic, global, superstructure optimisation for designing and operating the bioreactor. Optimisation approaches have been previously used to improve individual degrees of freedom in hollow fibre bioreactors (Chresand et al., 1988; Davidson et al., 2010; Shipley et al., 2011; Yoon et al., 2004), but our proposed bioreactor design and bioprocess optimisation simultaneously incorporates multiple degrees of freedom.

In this blood-producing bioreactor: nutrients, growth factors, and oxygen flow through the hollow fibres via Poiseuille flow and diffuse into the 3D polymeric scaffold. Resulting reactions cause the cells to grow, proliferate, and differentiate. Products and byproducts are excess cells and waste which diffuse out of the scaffold and exit through the hollow fibres. Design and operating choices include: (1) size/aspect ratio of the cylindrical bioreactor; (2) number of hollow fibres for delivering reactants and extracting products/byproducts; (3) flow rate of nutritious medium through the bioreactor; (4) medium composition, (5) oxygen concentration.

The bioreactor is modelled using the Krogh cylinder approximation (Krogh, 1919) diagrammed in Figures 4 and 5. Five species represent mass exchange in the bioreactor: glucose corresponds to cellular nutrients; lactate models waste; oxygen stands in for cellular metabolism; stem cell factor (SCF) represents cellular expansion; erythropoietin (EPO) is mapped to cellular differentiation. Mass transfer parameters are derived from prior work (Macedo, 2011; Panoskaltsis et al., 2012). Cellular growth, differentiation, and proliferation are modelled using the approach of Ma et al. (2007, 2012). The superstructure optimisation problem is formulated as a mixed-integer nonlinear program (MINLP) and solved to deterministic global optimality using ANTIGONE (Misener and Floudas, 2013a,b).

This paper considers the competitiveness of this blood-producing bioreactor with both typical and rare-blood transfusions. Section 2 reviews the literature; Section 3 describes the design decisions and model assumptions; Section 4 deduces model parameters; Section 5 develops the model as an MINLP; Section 6 solves the model and discusses the results; Section 7 concludes the manuscript by exploring the potential of globally-optimal superstructure design not only on this individual bioreactor but also more generally on bioprocess optimisation. As manuscript supplements: Appendix A records the stand-alone optimisation problem without any justification; Appendix B contains parameter values and defines all variables and parameters.

An earlier, shorter version of this manuscript appeared in Misener et al. (2014); this full-length paper includes detailed, quantitative justification for the design choices and augments the model to include bioreactor start-up via multiple quasi-steady states. Misener et al. (2014) propose robust optimisation for quantitatively assessing parametric uncertainties in this model, but the present manuscript is too long to incorporate complete uncertainty analysis; we limit ourselves to several *what-if* scenarios (§6.2) and parameter sensitivity analyses (§6.3). This effort belongs to the Imperial College *Framework for the Design, Modelling and Optimization of Biomedical Systems* (Velliou et al., 2014).

2. Literature Review

The *feasibility* of producing red blood cells (synonyms: RBC; erythrocyte) with close-to-physiological properties has been experimentally demonstrated by: Giarratana et al. (2005); Miharada et al. (2006); Olivier et al. (2006); Lu et al. (2008); Boehm et al. (2010); Timmins et al. (2011); Housler et al. (2012). The RBC produced by Giarratana et al. (2011) have been successfully injected into a human patient and feature: a circulation half-life of 26 days; proper cell enucleation; deformability characteristics only 9-17% different from native RBC; haemoglobin (*i.e.*, oxygen-carrying) capacity within $88 \pm 2.7\%$ of native RBC; correct expression of the surface protein CD235a (although over-expression of the surface protein CD71).

In vivo, CD235a is expressed $\approx 10^6\times$ per RBC; CD71 delivers iron to RBC progenitors for haemoglobin formation and is subsequently lost by the maturing cells.

But the *market viability* of *ex vivo* RBC remains uncertain with no successful commercialisation (Rousseau et al., 2014). Indeed, scaling up typical *ex vivo* RBC production techniques is commercially untenable; the most common method of RBC expansion in 2D static culture flasks would require 400 L of culture medium and $\approx$100 m^2 surface area to produce one unit of RBC (Timmins et al., 2011). Furthermore, the broader cellular therapy market is a fairly volatile industry where investors are typically wary (Mason et al., 2011). The high cost and long time scales associated with successful commercialisation of cellular therapies such as *ex vivo* red blood cell production requires careful cost-benefit analyses and detailed financial planning (Brindley et al., 2011).

RBC-producing bioreactors are a fiscally attractive alternative to 2D *ex vivo* RBC expansion techniques because cells can grow at higher concentrations in bioreactors and thereby reduce the required volume of culture medium (Rousseau et al., 2014). Doran et al. (2012), Housler et al. (2012), and Panoskaltsis et al. (2012) have each used hollow fibre bioreactors for red blood cell production. Hollow fibre bioreactors continuously deliver nutrients and clear waste from the bulk material via capillaries with porous walls. Mass transfer is convection-dominated within the hollow fibres and diffusion-dominated in the bulk; this design protects the cells growing in the bulk from shear stress while allowing them continuous access to nutrients.

Beyond allowing cells to grow and proliferate at higher concentrations, the hollow fibre bioreactor proposed by Panoskaltsis et al. (2012) and pictured in Figure 1 has two major design advantages: (1) the bulk material is a porous polyurethane (PU) scaffold mimicking the specialised 3D micro-environment structure of the bone marrow and (2) the dual hollow fibre design allows recycling the expensive growth factors in one set of capillaries while taking up nutrients discarding waste metabolites in another set of capillaries. As illustrated in Figure 1(b), nutrients enter and metabolites are cleared via the polyacrylonitrile hollow fibres (PAN HF; pore size ≈ 2 nm – 0.1μm); growth factors and mature cells are exchanged via the ceramic hollow fibres (CRM HF; pore size 1 – 2 μm).

Following prior art, we model mass transfer in the Panoskaltsis et al. (2012) bioreactor using the Krogh cylinder approximation (Krogh, 1919); consult Brotherton and Chau (1996) for a review of modelling hollow fibre bioreactors using the Krogh model. Mathematically optimising hollow fibre bioreactors is more rare: Chresand et al. (1988) mathematically optimise hollow fibre spacing; Willaert et al. (1999) vary individual design parameters to improve bioreactor performance; Yoon et al. (2004) propose an algorithm for sequentially designing a hollow

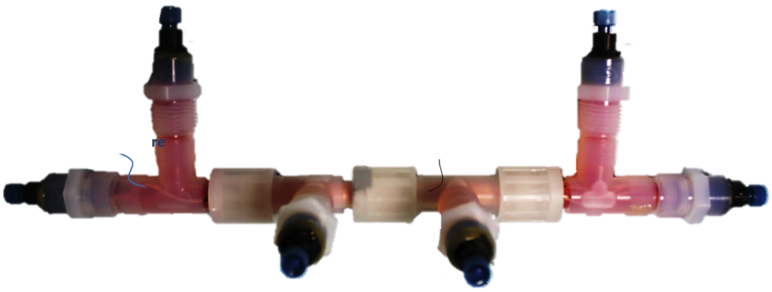

(a) Bioreactor within plastic housing; exit ports are for initialising the culture and mass exchange

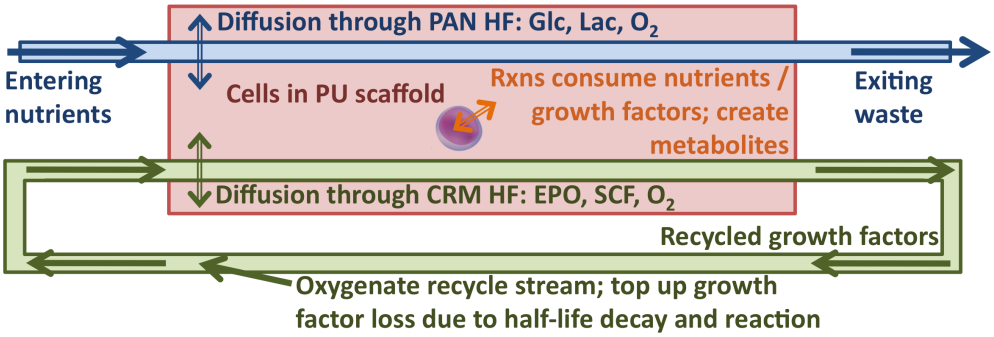

(b) Mass transfer within the Bioreactor

Figure 1: Bioreactor superstructure (Panoskaltsis et al., 2012)

fibre bioreactor; Davidson et al. (2010) graphically represent the feasible operating regimes; Shipley et al. (2011) vary operating conditions to find a feasible solution. All of the preceding approaches assume steady-state operating conditions in the hollow fibre bioreactor; none exploit the known advantages of simultaneously integrating many design choices via mathematical optimisation strategies.

We cannot accurately assume steady state operation; representing cellular growth, proliferation, and differentiation requires modelling multiple operation phases (including start-up) with a dynamic model. To create an MINLP, we discretise the ordinary differential equation (ODE) model of haematopoiesis (*i.e.*, blood production) introduced by Colijn and Mackey (2005) and extended by Ma et al. (2007, 2012). Recall that optimising a bioreactor by discretising a dynamic optimisation problem and solving the resulting MINLP has been previously proposed by Banga et al. (1998, 2005). The mathematical novelty of our approach stems from: (1) explicitly considering bioreactor design; (2) incorporating a mathematical model of haematopoiesis into the optimisation problem. The engineering contribution is to show how this superstructure design strategy can generally impact bioprocess optimisation. The industrial contribution is to show, for the first time, the potential for *ex vivo* red blood cell production to compete openly

against the transfusion market for rare blood.

3. Design Decisions and Model Assumptions

Starting with the Panoskaltsis et al. (2012) bioreactor, the available design decisions are:

- **Number of equivalent bioreactors:** Producing one unit of RBC ($\approx 2 \times 10^{12}$ cells) requires *parallelising* the process rather than scaling it up. A narrow bioreactor may have better mass transfer from the capillaries to the bulk than a wide reactor (area scales with radius squared); we have experimentally deduced physical limits on reactor length (see Table B.9). A single bioreactor may not meet production needs; the optimisation model selects the number of equivalent reactors.
- **Size / aspect ratio of a bioreactor:** Table B.9 gives physically plausible ranges for bioreactor size, the optimisation model selects the actual values.
- **Number / type of hollow fibres:** Panoskaltsis et al. (2012) describe two possible hollow fibres running through the bioreactor; the *polymeric* capillaries deliver nutrients and clear waste while the *ceramic* membranes deliver the expensive growth factor proteins. The optimisation model selects the number and type of each hollow fibre.
- **Cellular Inoculum:** The optimisation model selects the quantity of umbilical cord blood (UBC) to inoculate the scaffold in the bioreactor initialisation phase (Macedo, 2011).
- **Flow rate through the reactor:** Table B.9 lists ranges for flow rates based on hollow fibre material properties reported by Macedo (2011).
- **Composition of the medium:** The model selects the optimum concentrations of: glucose; lactate; EPO; O_2; SCF

Before deducing the parameters in Section 4 and assembling the optimisation model in Section 5, Table 1 states our model assumptions and justifies them. The mass transfer and homogeneity assumptions are typical for a Kroghian cylinder approximation (Brotherton and Chau, 1996; Jayaraman, 1992; Kreuzer, 1982; Labecki et al., 1996), but it is still important to justify them for the bioreactor of Panoskaltsis et al. (2012).

This manuscript builds an optimisation model based on nominal reactor performance rather than accounting for known uncertainty as in Misener et al. (2014); this is to carefully justify all design decisions. But all assumptions in Table 1 are subject to uncertain behaviour. For example, Panoskaltsis et al. (2012) have characterised not just material properties but also coefficient

variability. Species reaction rates and cellular kinetics are also subject to uncertainty. Several of the model assumptions are quite safe (*e.g.*, HF capillaries will always have a much smaller radius than transverse length). But other assumptions are more risky; we discuss in Table 2 the implication of key model assumptions being violated and how to quantify or mitigate risk.

Table 1: Model Assumptions

Assumption	Justification
Conditions are equal from bioreactor to bioreactor	Bioreactors operate in parallel; this assumption is based on average expected values rather than an assertion of homogeneity
Cylindrical reactor geometry	Macedo (2011) describes a design protocol leading to a cylindrical bioreactor
Constant flow rates in the bioreactor	The range of possible capillary flow rates will not shear RBC (see Section 5.3.1); flow rates are always the maximum allowed by the physical capillary properties to promote mass transfer
Parabolic, Poiseuille flow in the hollow fibre	Section 5.3.2 shows that the flow is laminar; capillary cross-section is a circle (Panoskaltsis et al., 2012)
Isotropic conditions	The bioreactor operates in a temperature-controlled incubator; reactions are not appreciably exo- or endothermal
Known geometry and mass transfer coefficients	Material properties for both the HF and PU scaffold are characterised by Panoskaltsis et al. (2012)
Homogeneously distributed capillaries	Required for Krogh cylinder approximation (Section 5.3.3); based on expected values rather than an assertion of homogeneity
No axial flow in the HF membranes or PU scaffold	Transport is diffusion-dominated in the PU scaffold and HF membrane; transport is convection-dominated in the HF lumen. We ignore axial diffusion in the PU scaffold and HF membrane because diffusion rates are $> 10^3\times$ smaller than axial flow rates in the HF lumen
The fibre and the Krogh radii are much smaller than the fibre length	Table B.9 shows that capillaries are $> 100\times$ smaller than the smallest possible bioreactor length; the largest possible reactor radius is $\approx 10\times$ smaller than the smallest possible bioreactor length; Further analysis of entrance effects is in Section 5.3.2

continued on the next page

Table 1 (Model Assumptions) continued

Assumption	Justification
Reaction is inert in both the hollow fibre and the membrane	Cells in a capillary will flow out the reactor; RBC may deform and squeeze through the hollow fibre membrane but will not comfortably reside there (Macedo, 2011).
Zero order reaction	Insufficient access to nutrients and growth factors will stress cells; patterns of growth, proliferation, and differentiation will change. Assume that cells consume their desired amount of nutrients until nutrients unavailable; no cells live outside that region
Fickian diffusion with a constant diffusion coefficient for all species	No chemical interactions between species in the feed and the HF membrane or the PU scaffold; No membrane fouling after 30 days experiment in Macedo (2011)
All cell types are evenly and equally distributed across a bioreactor	This assumption is based on average expected values rather than an assertion of homogeneity; it is ameliorated by using the 4 discrete quasi-steady states described in Section 5.5
Homogeneous species consumption/production	As above, this assumption is based on average expected values and ameliorated via the 4 discrete quasi-steady states
Known inlet/outlet species concentrations	Directly experimentally measurable
Glucose represents cellular nutrients	In *ex vivo* culture, glucose is the primary energy supply (Mulukutla et al., 2010); glucose and glutamine are the two molecules appreciably catabolised in mammalian cell culture but glucose is typically used first (Heiden et al., 2009)
Lactate represents cellular waste	Data of Macedo (2011) shows that lactate is the first waste product to significantly build up in the reactor
O_2 represents metabolism	As in most HF bioreactors, O_2 is limiting
SCF represents cell proliferation	Stem-cell self-renewal depends on the presence of SCF (Cabrita et al., 2003); c-Kit (CD117), the SCF receptor, is present in stem cells and is typically lost during differentiation, SCF promotes proliferation and early differentiation of multipotent stem cells (Lennartsson and Ronnstrand, 2012)

continued on the next page

Table 1 (Model Assumptions) continued

Assumption	Justification
EPO represents cell differentiation to the erythrocyte lineage	EPO is required for erythroid lineage commitment; knock-out mice missing the EPO receptor cannot make RBC (Wu et al., 1995)
Only RBCs and other terminally-differentiated cells exit the bioreactor	Precursor cells likely attach themselves to the 3D PU scaffold via adhesion proteins (Mortera-Blanco et al., 2011); mature cells will be more mobile in the biomimetic reactor
Reactor has 4 quasi-steady states	The bioreactor can operate up to 28-35 days; the maximum possible cellular population doubling time is 5 days. ODEs of cellular kinetics are discretised into 4 time periods correlated to data of Mortera-Blanco et al. (2011); see Section 4.5
There are 4 types of cells in the reactor	Similar to Colijn and Mackey (2005), we coarse-grain the cellular types in the reactor based on the stem cell progenitors and the 3 most common cell lineages; see Section 4.4

Table 2: Implication of key model assumptions being violated and how to check or mitigate violation in the key model assumptions

Implication if Violated	How to Check / Mitigate
Assumption: Homogeneous performance *Conditions are equal from bioreactor to bioreactor; homogeneous species consumption / production; all cell types are evenly and equally distributed across a bioreactor*	
Variability may imply that a fraction of bioreactors fail; analysis in this manuscript neglects the fail fraction for lack of data which could be used to scale bioreactor costs.	Quality by Design testing for determining the probability of bioreactor failure.
Assumption: Homogeneously distributed capillaries	
Our computational fluid dynamics analysis (data not shown) demonstrates that 3D modelling for heterogeneously distributed capillaries induces mass transfer characteristics diverging 10 – 20% from the Kroghian model.	Allow 10 – 20% uncertainty in the mass transfer parameters.

continued on the next page

Table 2 (Checking Model Assumptions) continued

Implication if Violated	How to Check / Mitigate
Assumption: Zero order reaction	
This assumption is incorrect; each cell type will have a higher-order reaction with each species. The inaccuracy will increase the parameter uncertainty.	Allow uncertainty in rxn rates; adding parameters complicates without more accuracy.
Assumption: Can describe reactor behaviour using 5 representative species *Glucose represents cellular nutrients; lactate represents cellular waste; O_2 represents metabolism; SCF represents cell proliferation; EPO represents cell differentiation to the erythrocyte lineage*	
May be disregarding mass transfer for a limiting species; not capturing erythropoiesis with complete accuracy.	Design of Experiments to see if range expected values in other species impacts bioreactor performance
Assumption: Only RBCs and other terminally-differentiated cells exit the bioreactor	
Progenitor cells exiting the bioreactor would change the number of cells available for proliferation and differentiation.	Quality by Design testing
Assumption: Erythropoiesis model is correct *Reactors have 4 quasi-steady states; there are 4 types of cell lineages in the reactor*	
Bioreactor may not produce as many RBC as expected; growth factor feeding schedule may be incorrect	Substitute competing models of erythropoiesis (*e.g.* Lobato da Silva et al., 2003); test variance

4. Deducing the Parameters

This section discusses nominal parameter values for the Section 5 model. Section 4.1 describes the relevant financial costs; Section 4.2 quantifies the acceptable concentration ranges of each species; Section 4.3 calculates the mass transfer parameters; Section 4.4 delineates the start-up conditions; Section 4.6 describes the reaction rates; Section 4.5 gives associated cellular kinetics. We record the uncertainty associated with each parameter for the Section 6.3 sensitivity analysis; the parameter ranges would also be useful in a robust optimisation framework (Misener et al., 2014).

4.1. Nutrient and Growth Factor Costs

The National Health Service (NHS) spends an average of £125 per unit of RBC; this includes costs of: collection, testing, storage, transportation, distribution (Lawes, 2011). The additional costs associated with manufacturing RBC include: nutrients and specialised growth factor proteins, bioreactor materials, incubator equipment to maintain the *ex vivo* culture at proper conditions, staff time to initiate and tend the culture. We also consider the cost of acquiring precursor cells that are subsequently expanded in the bioreactor.

A unit of rare blood has an average cost of $1150 to $3025 in the USA and may reach £25k per patient episode in the UK (Meny et al., 2013; Whitaker and Henry, 2011). Therefore, all additional costs have to be on the order of $2000 to compete openly with the rare blood transfusion market; costs an order of magnitude larger can still compete with the rarest cases.

Timmins and Nielsen (2009) show that the dominant costs of manufacturing RBC are the nutrients and specialised growth factor proteins; they further show that it is the growth factors in general and SCF and EPO in particular contribute to more than half the total manufacturing cost. Therefore, we limit our cost analysis to three items; for comparison to the pricing of Timmins and Nielsen (2009), we use identical costing:

1. EPO (Erythropoietin): 0.023 US $/U (Timmins and Nielsen, 2009)
2. SCF (Stem Cell Factor): 320 US $/mg (Timmins and Nielsen, 2009)
3. Umbilical Cord Blood (UCB) from the NHS: US $ 369 for 4×10^8 nucleated cells; US $ 243 for $0.5 - 2.0 \times 10^8$ nucleated cells (NHS, 2013)

EPO and SCF prices are considered because they are the most relevant to RBC expansion; UCB prices are considered so that the optimisation model will not select the non-physical solution of no proliferation by just suggesting differentiation of one haematopoietic stem cell (HSC) into one RBC. As is obvious from the price of the NHS UCB, meeting the financial goals requires $> 10^3 \times$ expansion during differentiation from HSC to RBC.

Other growth factors or cytokines have to be in the cocktail; haematopoiesis in general and erythropoiesis in particular is tightly regulated by a group of early-acting cytokines including: interleukin-1 (IL-1); interleukin-3 (IL-3); interleukin-6 (IL-6); granulocyte-macrophage colony-stimulating factor (GM-CSF); SCF (Metcalf, 2008). Later-stage erythropoiesis depends on growth factors including: EPO; IL-3; GM-CSF; SCF; thrombopoietin (TPO) (Metcalf, 2008). Ideal engineering design would provide optimal, time-varying cytokines concentrations for the culture duration, but scientists have not yet untangled the contribution of each signalling protein to erythropoiesis.

Table 3: Acceptable Species Concentration Ranges (Chow et al., 2001; Mantalaris et al., 1998; Ozturk et al., 1997; Slyke and Neill, 1924; Wodnar-Filipowicz et al., 1993; Yeo et al., 2013)

	Species	$\hat{C}_{k,\mathrm{IN}}$	$C_{k,\mathrm{MIN}}$	$C_{k,\mathrm{MAX}}$	Units
EPO	Erythropoeitin	–[†]	2×10^4	–	$\mathrm{U/m^3}$
Glc	Glucose	25	0.3	–	$\mathrm{mol/m^3}$
Lac	Lactate	0.00	–	22	$\mathrm{mol/m^3}$
O_2	Oxygen	0.26	0.026	–	$\mathrm{mol/m^3}$
SCF	Stem Cell Factor	–[†]	3.3	–	$\mathrm{mg/m^3}$

[†] Macedo (2011) added EPO and SCF as a pulse, not continuously

This manuscript could be updated to incorporate additional species based on new understanding. For now we justify our design choices by observing that SCF for proliferation and EPO for differentiation can almost completely describe *in vitro* erythropoiesis (Wang et al., 2008). SCF and EPO are the two most prominent factors required for the *in vitro* growth of erythroid progenitor cells (Panzenbock et al., 1998) and the *only* two cytokines used in the successful RBC expansion experiment of Macedo (2011).

4.2. Acceptable Concentration Ranges of the Species

Hollow fibre bioreactors are often modelled and optimised only with respect to the mass transfer of O_2; O_2 is typically the limiting substrate. But the dual hollow fibre design of Panoskaltsis et al. (2012) and our goal of directly considering financial costs requires considering five species. As described in Section 3, the model incorporates: glucose; lactate; O_2; SCF; EPO. This section justifies acceptable concentration ranges for each of the five species; Table 3 reports the conclusions of this analysis.

Glucose / Lactate: The minimum allowable level of the nutrient glucose and the maximum allowable level of the waste product lactate is based on the experimental analyses of Macedo (2011) and Yeo et al. (2013).

Oxygen: The range of O_2 concentrations in human bone marrow (BM) favour differentiation into many disparate cell types (Chow et al., 2001); our analysis is on aggregate behaviour. Physiological O_2 in the BM ranges 2–6% (Cabrita et al., 2003), but transfer is less effective in the bioreactor because there are many fewer HF than arteries and capillaries in the BM (Beutler et al., 2001). We permit 2–20% O_2 (0.026 – 0.26 $\frac{\mathrm{mol}}{\mathrm{m^3}}$) to get a better driving force; this is the range between lower physiological levels and atmospheric concentration.

Stem Cell Factor (SCF) is a 18.5 kDa cytokine that forms a dimer in water. A typical SCF culture value is 50 ng/mL (Mantalaris et al., 1998). Based on the cytokine-free results of Mortera-Blanco et al. (2011), we hypothesize that the bioreactor can function at typical physiological serum levels, 3.3 ng/mL (Wodnar-Filipowicz et al., 1993; Langley et al., 1993)

Erythropoetin (EPO) is a 34 kDa glycoprotein typically measured in units U ($1.29 \times 10^5 \frac{\text{U}}{\text{mg}}$). Mantalaris et al. (1998) showed that long-term, sustained erythroid development in 3D culture favours a low EPO level (≈0.2 U/mL when the typical 2D culture value is 2 U/mL). Based on the cytokine-free results of Mortera-Blanco et al. (2011), we hypothesise that the bioreactor can function at physiological serum levels, ≈20 mU/mL (Kaushansky, 2006).

The growth factors (EPO; SCF) are supplied exogenously, but there may be endogenous cytokine production (Mahaffy et al., 1998). But Macedo (2011) found both SCF and EPO to be beneath the detection limit when using both an Human SCF Quantikine ELISA Kit (R&D Systems; #DCK00; minimum detection 3.12×10^{-2} mg/m^3 or 1% of the minimum SCF required by the bioreactor) and an Human Erythropoietin Quantikine IVD ELISA Kit (R&D Systems; #DEP00; minimum detection 2.5 mU/mL or 10% of the minimum required EPO); we therefore ignore endogenous cytokine production for the purposes of this manuscript.

We also have to consider half-life of the growth factor proteins; the *in vitro* half-life of EPO and SCF is 72[1] and 48 (Kishimoto et al., 2010) hours, respectively. These durations are significantly longer than the known *in vivo* half-lives (Eckardt et al., 1989; Elliott et al., 2008; Drouet et al., 2004) because growth factors may be cleared *in vivo* by the kidney, liver, or bone marrow.

4.3. Mass Transfer Parameters

Table B.9 lists mass transfer parameters derived from the work of Macedo (2011) and Panoskaltsis et al. (2012). This section quantifies the diffusivity of each species in: (1) the HF lumen; (2) the HF membrane; (3) the PU scaffold; the outcome of this analysis is listed in Table 4.

The diffusivities of glucose, lactate, and O_2 in the lumen is approximated as the diffusivity of that species in water (Curcio et al., 2005; Chow et al., 2001; Dutta and Popel, 1995; Ribeiro et al., 2005). We assume that EPO and SCF have diffusion coefficients in water that can be modelled (Young et al., 1980):

$$D_{k,W} = 8.34 \times 10^{-8} \frac{T}{\eta M^{1/3}}, \tag{1}$$

[1] An NHS pharmacist advised us that *the patient may ... store [EPO] at room temperature for up to three days*

Table 4: Diffusivities of each species k in each region i (Curcio et al., 2005; Macedo, 2011; Maxwell, 1881; Ribeiro et al., 2005; Young et al., 1980)

Species	Region Diffusivities [$\frac{m^2}{s}$]	
	HF Lumen	PU Scaffold
Glc	$9.24 \pm 0.15 \times 10^{-10}$	$8.39 \pm 0.52 \times 10^{-10}$
Lac	$9.93 \pm 0.15 \times 10^{-10}$	$9.01 \pm 0.54 \times 10^{-10}$
O_2	3.29×10^{-9}	$2.98 \pm 0.13 \times 10^{-9}$
EPO	$1.09 \pm 0.22 \times 10^{-10}$	$0.99 \pm 0.25 \times 10^{-10}$
SCF	$1.34 \pm 0.27 \times 10^{-10}$	$1.21 \pm 0.30 \times 10^{-10}$

$\varepsilon_{HF} = 0.8$; PAN Exchange: Glc, Lac, O_2;
CRM Exchange: EPO, SCF, O_2

where T is the absolute temperature (310.2 Kelvin); η is the viscosity of water (0.69 $\frac{kg}{m\ s}$ at 310.2 Kelvin); M is the molecular weight of the protein ($M_{EPO} = 34$ kDa; $M_{SCF} = 18.5$ kDa). Therefore we have: $D_{EPO,W} = 1.09 \pm 0.22 \times 10^{-6} \frac{cm^2}{s}$; $D_{SCF,W} = 1.34 \pm 0.27 \times 10^{-6} \frac{cm^2}{s}$. Young et al. (1980) claim that their method is accurate within 20%; hence the error bars. In Table 4, the error bars on the scaffold diffusivities are based on both the error in the water measurement and the error in the porosity.

The diffusivities in the PU scaffold are estimated (Maxwell, 1881):

$$D_{k,3} = \frac{2\, D_{\text{water},k}}{3 - \varepsilon_{PU}};\ k \in \{\text{Glc, Lac, } O_2\text{, EPO, SCF}\} \tag{2}$$

The porosity of the scaffold is: $\varepsilon_{PU} = 0.791 \pm 0.1$ which implies that the diffusivity in the scaffold is: $D_{Glc,3} = 8.39 \pm 0.52 \times 10^{-10} \frac{m^2}{s}$; $D_{Lac,3} = 9.02 \pm 0.54 \times 10^{-10} \frac{m^2}{s}$; the error is propagated from the known uncertainty of the scaffold.

We assume that the porosity of both the polymeric and ceramic HF is $\varepsilon_{HF} = 0.8$. The PAN polymeric HF allow exchange of: Glc; Lac; O_2. The CRM HF permit exchange of: EPO; SCF; O_2. Practically, there will also be glucose and lactate exchange in the ceramic membrane, but we assume that the liquid in the recycle stream is in equilibrium with the scaffold bulk so that nutrient and metabolite exchange is negligible.

4.4. Cell Types and Start-Up Inoculum Conditions

It is not mathematically practical to simultaneously consider the many heterogeneous proliferating and differentiating cell types in the bioreactor, so we simplify our analysis to four cell types. We assume that the distribution of cells in the bioreactor is uniform for each of four

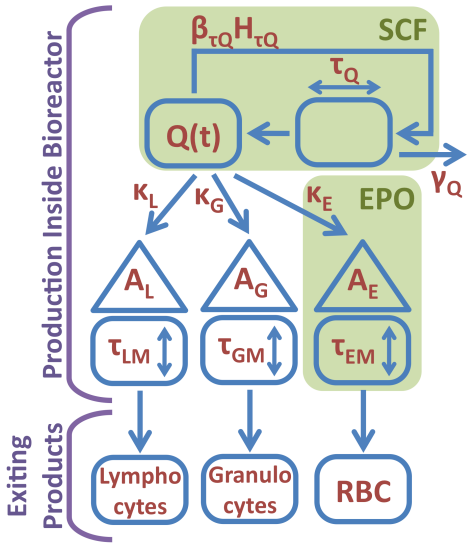

Figure 2: Cellular proliferation and differentiation (Colijn and Mackey, 2005; Ma et al., 2012)

haematopoietic cell types H illustrated in Figure 2: dividing cells $H_{Q,t}$ (*e.g.*, haematopoietic stem cells), erythrocytes and maturing erythrocytes $H_{E,t}$, granulocytes and monocytes $H_{G,t}$, and lymphocytes $H_{L,t}$. Our choice of representative cells is similar to Colijn and Mackey (2005) and Ma et al. (2012) in that we consider three cell types: HSC, erythrocytes, and lymphocytes. The difference is that we are considering an aggregate of granulocytes and monocytes as the fourth compartment rather than platelets; granulocytes and monocytes are significant components of our bioreactor that consume the reactants oxygen and glucose and produce metabolites such as lactate whereas platelets will exit the reactor like RBC.

We assume that the bioreactor is initialised with nucleated cells from UBC as outlined in Table 5 so that expected cell numbers at time zero are: $H_{Q,0} = 35.80 \times 10^6$ cells per cord; $H_{E,0} = 0$ cells per cord; $H_{G,0} = 300.85 \times 10^6$ cells per cord; $H_{L,0} = 249.34 \times 10^6$ cells per cord.

4.5. Cell Kinetics: Growth; Proliferation; Differentiation

A healthy adult with 70kg body weight typically has a BM cellular density up to 5×10^8 cells/mL (Peng and Palsson, 1996) and an RBC production rate of 0.1 blood units/day (2×10^{11} cells/day); this can increase $10\times$ under stress (Timmins and Nielsen, 2009). In normal tissue, the surface area of capillaries per organ mass is $2\text{mm}^2/\text{g}$ assuming blood irrigation by capillaries with 10 μm diameter and a blood average velocity of 0.1 $\frac{\text{cm}}{\text{s}}$ (King, 2005; Macedo, 2011); the surface area increases in cancer (Schlageter et al., 1999).

The BM is $\approx 5\%$ of total body weight or 3650 g for a healthy adult man; approximately 1170

Table 5: Absolute Number of Cells after Umbilical Cord Blood Processing (n = 80); Total Cell Number is 582.51×10^6 *(Basford et al., 2010)*

Cell Type	FACS Phenotype	Cell # ($\times 10^6$)	FACS (%)
Lymphocytes	$CD45^+$ / $CD14^-$	249.34	37.09
Monocytes	$CD45^+$ / $CD14^+$	67.23	9.05
Granulocyte	$CD45^+$ / $CD14^-$	233.62	50.27
HSC	$CD45^+$ / $CD34^+$	35.80	4.54

Due to double counting: individual cell no. sum to greater than 582.51×10^6
FACS: fluorescence-activated cell sorting; HSC: haematopoietic stem cell

Table 6: Experimental Bioreactor Data (Macedo, 2011); Calculated Reaction Rate

Species	$\hat{C}_{k,\mathrm{IN}}$ $[\mathrm{mol/m^3}]$	$\hat{C}_{k,\mathrm{OUT}}$ $[\mathrm{mol/m^3}]$	V_k $[\mathrm{mol/m^3/day}]$
Glc	25	19.9 ± 2.1	$2.41 \pm 0.99 \times 10^{-5}$
Lac	0	13.5 ± 5.2	$-6.39 \pm 2.46 \times 10^{-5}$

g in men and 900 g in women is haematopoietically active (Hindorf et al., 2010). Mass density of active BM is 1.03 g/cm^3 (Pichardo et al., 2007), so we estimate a volume of 10^6 mm^3 in the BM for growing cells. In contrast, the volume of the Panoskaltsis et al. (2012) reactor is 2109 mm^3. If the bioreactor operated exactly like the bone marrow, then we would require on the order of 500 bioreactors to make blood at normal physiological rates. Under stress, bone marrow can operate at roughly $10\times$ the normal rate; this would be the volume equivalent of 50 bioreactors. So, by order of magnitude analysis, we expect 50–500 reactors if we wish to make blood at physiological rates.

We assume that the maximum cellular possible doubling time is 5 days and that a cell cycle is $\approx$ 24 hours long; this approximation is justified by the maximum proliferation potential seen *in vivo* for stem cells and cancer (Rew and Wilson, 2000; Riccardi et al., 1988). Using the convention of Colijn and Mackey (2005), the maximum number of cells that can be actively proliferating at any one time is 14.9%. We model cellular growth, differentiation, and proliferation using an appropriate adaptation of the models of Colijn and Mackey (2005) and Ma et al. (2012); these changes are to interlink the presence of SCF and EPO with cellular kinetics.

Table 7: Cellular parameters of individual cell types in the bone marrow haematopoietic compartment (Chow et al., 2001)

Parameter	Erythro-cytes	Lympho-cytes	Granulo-cytes	Mono-cytes	Megakaryo-cytes	Adipo-cytes
Fraction of Cells	3.46–37.6	2.5–25	16.9–100	0–4.3	0–3	0
Average Cell Diameter (μm)	7.35	14.5	17.5	31.0	95.0	175.0
Specific Cell Vol $\times 10^9$ ($\frac{\text{cm}^3}{\text{cell}}$)	0.208	1.60	2.80	15.6	448.90	2806.0
Specific O_2 Uptake Rate $\times 10^{15}$ ($\frac{\text{mol}_{O_2}}{\text{cell day}}$)	38.88–155.76	16.8–1200	528–15576	528–15576	34560	7776
Vol O_2 Rxn Rate $\times 10^9$ ($\frac{\text{mol}_{O_2}}{\text{cm}^3\ \text{s}}$)	2.2–8.7	0.1–7.1	2.2–64.4	0.4–11.6	0.89	0.03

Interval corresponds to differences between progenitor and mature cells

4.6. Reaction Rates

To find the reaction rate of glucose and lactate in the scaffold, we assume that the reaction within a bioreactor was zeroth order and calculate the consumption rate per reactor unit volume:

$$V_k = \frac{\hat{U}_Z \cdot \left(\hat{C}_{k,\text{IN}} - \hat{C}_{k,\text{OUT}}\right)}{\hat{L}} \quad \forall k \in \{\text{Glc}, \text{Lac}\} \tag{3}$$

where $\hat{L} = 150$ mm and $\hat{U}_Z$; $\hat{C}_{k,\text{IN}}$; $\hat{C}_{k,\text{OUT}}$ are taken from experimental data summarised in Table 6 (Macedo, 2011). The calculations yield: $V_{\text{Glc}} = 2.41 \pm 0.99 \times 10^{-5} \frac{\text{mol}}{\text{m}^3\ \text{day}}$; $V_{\text{Lac}} = -6.39 \pm 2.46 \times 10^{-5} \frac{\text{mol}}{\text{m}^3\ \text{day}}$. Table 7 records the O_2 consumption rates of cells assembled by Chow et al. (2001); note that there is a range for each cell type. In every case we will assume that immature cells consume the lower and mature cells the higher end; this is in line with experimental observation (Vlaski et al., 2009).

Although there is not a total dependence on SCF for erythropoiesis and erythropoietin can support erythropoiesis in the absence of a functional SCF receptor c-Kit (Lennartsson and Ronnstrand, 2012), stem-cell self-renewal depends on the presence of SCF (Cabrita et al., 2003). SCF-mediated proliferation of HSC increases the pool of HSC available for later differentiation into RBC. But SCF and its receptor c-Kit have not been characterised as carefully as EPO/EPOR. It is known that c-Kit expression is highest in erythroleukaemia cell lines with

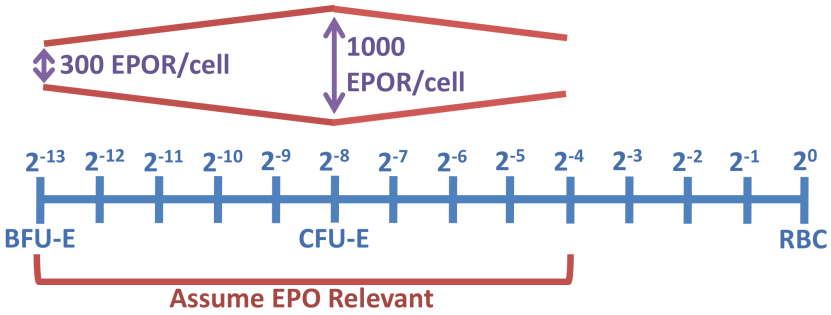

Figure 3: Assume that EPO is relevant from BFU-E stage to just past CFU-E stage (Terszowski et al., 2005; Lodish et al., 2010)

up to 5 – 10 $\times 10^4$ c-Kit receptors per cell (Broudy, 1997). In acute myeloid leukaemia, the number of high-affinity SCF receptors on one cell was found to range between 210 – 2860 (Broudy et al., 1992). c-Kit is a high-affinity receptor for SCF, the dissociation constant k_d is 50 - 200 pmol/L (Broudy, 1997). But, by order of magnitude analysis and biomimicry, there will always be many fewer HSC cells than other cell types. We are therefore ignoring loss of SCF due to consumption in a reaction; this is in line with experimental results of Macedo (2011).

Figure 3 illustrates our model of EPO reaction with the EPO receptor (EPOR). As HSC mature in the erythroid lineage, and pass from the early-stage erythroid burst-forming unit (BFU-E) to intermediate-stage BFU-E, they acquire high-affinity EPOR surface markers (≈ 300) (Adamson, 1994). In the 4-5 cell divisions from BFU-E to erythroid colony-forming unit (CFU-E), cells acquire more high-affinity EPOR receptors (Terszowski et al., 2005). Most of the EPOR is lost by the proerythroblast phase; the maturation of proerythroblasts to enucleated erythrocytes in 3-4 cell divisions is EPO-independent (England et al., 2011). Overall, there are 9-16 cell divisions from BFU-E's to erythrocytes (Hattangadi et al., 2011), so we assume: (1) 5 divisions from BFU-E to CFU-E; (2) 4 divisions from CFU-E to proerythroblast; (3) 4 divisions from proerythroblast to enucleated RBC.

To quantitate the EPO/EPOR reaction, the enzyme dissociation constant k_d is defined:

$$k_d = \frac{[\text{EPO}] \cdot [\text{EPOR}]}{[\text{EPO} \bullet \text{EPOR}]} \tag{4}$$

Using $k_d = 0.43$ U / mL (Adamson, 1994; Youssoufian et al., 1993) and physiological condi-

tions $[\text{EPO}] = 0.02$ U / mL (Mantalaris et al., 1998), we get:

$$\frac{[\text{EPO} \bullet \text{EPOR}]}{[\text{EPOR}]} = 4.65 \times 10^{-2} \tag{5}$$

There are approximately 300-1000 high-affinity EPO receptors on BFU-E and CFU-E cells (Adamson, 1994; Youssoufian et al., 1993); the receptors monotonically increase from 300 EPO receptors on BFU-E to 1000 EPO receptors on CFU-E and back to 300 receptors just before becoming proerythroblasts (Terszowski et al., 2005; Lodish et al., 2010). In physiological conditions, there will be $0.0465 \cdot 300 = 13.9$ to $0.0465 \cdot 1000 = 46.4$ receptor / growth factor complexes. Becker et al. (2010) show that approximately 80% of the EPO-EPOR complexes will be taken into the cell via endocytosis; this implies that approximately 11.3 – 37.2 EPO molecules are consumed per cell division. As shown in Figure 3, we are estimating that EPO is relevant for BFU-E and CFU-E cells; 1 RBC is equivalent to:

$$\frac{\sum_{i=0}^{5} 2^i \cdot \left(11.3 + \frac{i}{5} \cdot (37.2 - 11.3)\right) + \sum_{i=6}^{9} 2^i \cdot \left(37.2 + \frac{i-5}{4} \cdot (11.3 - 37.2)\right)}{2^{13}} = 2.1 \tag{6}$$

EPO molecules. This result is highly dependent on the number of cell divisions from proerythroblasts to RBC; if there are only 11 rather than 13 cell divisions then then we need 8.5 EPO molecules. Also, recall that reaction rates for SCF and EPO are conflicting in the literature; alternative analysis is available, for example, in Koller et al. (1995) and Sensebe et al. (1997). The 3D versus 2D construction of the bioreactor legitimates our choice of literature sources.

5. Model Development

This model minimises cost in a bioreactor producing one unit of red blood cells while providing sufficient (*i.e.*, critical) nutrient delivery and waste disposal. As described in Section 3, operating choices include: (1) number of equivalent bioreactors N_{R}; (2) size and aspect ratio R_4 by L of the cylindrical bioreactor; (3) number of polyacrylonitrile (PAN; $N_{\text{HF,PAN}}$) and ceramic ($N_{\text{HF,CRM}}$) hollow fibres for delivering reactants and extracting products and by-products; (4) quantity of umbilical cord blood (UBC) to initialise the scaffold; (5) flow rate of nutritious medium U_Z through the bioreactor; (6) medium inlet composition $C_{k,\text{IN}}$ for $k \in \{\text{Glucose, SCF, EPO}\}$, (7) ambient oxygen concentration $C_{\text{Oxygen,IN}}$.

This section develops the model based on the analysis in Section 4; all indices, variables, and parameters are defined in Table B.9. The entire model is also reported in Appendix A.

5.1. Objective

The objective is minimising bioreactor cost while providing sufficient (*i.e.*, critical) nutrient delivery and waste disposal. We assume that the contributions to bioreactor cost are represented by growth factors and UCB cellular inoculum; we neglect the price of (1) nutrients; (2) bioreactor materials and fabrication; (3) operator time; (4) product transportation and storage. Just considering growth factor costs would be consistent with Timmins and Nielsen (2009), but for mathematical optimisation we also need to consider UBC initialisation costs; otherwise the model will suggest an impractically expensive inoculum requiring very little growth factors.

$$\begin{aligned} \min \quad & \left[\sum_{k \in \{\text{EPO; SCF}\}} p_k \cdot \tau_k \cdot N_{\text{R}} \cdot \text{Vol}_{\text{Recyc}} \cdot C_{k,\text{IN}} + p_k \cdot D \cdot V_k \cdot \text{Vol}_T \right] \\ + & \left[\sum_{h \in \{Q; E; G; L\}} p_{\text{UCB}} \cdot H_{h,0} \cdot \text{Vol}_T \right] \end{aligned} \tag{7}$$

The growth factor costs are continuous and scale with the price p_k of the growth factors entering each of the equivalent N_{R} reactors. The two contributions to growth factor cost are protein half life decay and reaction depletion. To calculate the half life decay, $\text{Vol}_{\text{Recyc}}$ is the volume needed for flowing through the reactor plus recycle storage; τ_k is the replenishment coefficient calculated in Eq. (45); $C_{k,\text{IN}}$ is the entering concentration. For the reaction: V_k is the maximum reaction rate representing the zero-order reaction limit; D is the time the reactor is run in days; Vol_T is the total scaffold volume. For the initialisation price: p_{UCB} is the price of UCB per cell and the sum of $H_{h,0}$ represents the total cell concentration at time zero.

5.2. Superstructure Topology

N_{R} bioreactors are parallelised to create one unit of red blood cells; each of the N_{R} bioreactors is a cylinder with aspect ratio R_4 by L and N_{HF} hollow fibres. The flow develops after entry length L_e. The N_{HF} hollow fibres are further divided into $N_{\text{HF,PAN}}$ PAN hollow fibres and and $N_{\text{HF,CRM}}$ ceramic hollow define equivalent Krogh Cylinders (Krogh, 1919).

Hollow fibre distribution: Each bioreactor has N_{HF} PAN or ceramic hollow fibres:

$$N_{\text{HF}} = N_{\text{HF,PAN}} + N_{\text{HF,CRM}} \tag{8}$$

Packing hollow fibres into a bioreactor: There is a maximum physical density for packing cylinders into larger cylinders; we estimate from experiments that this density to be approxi-

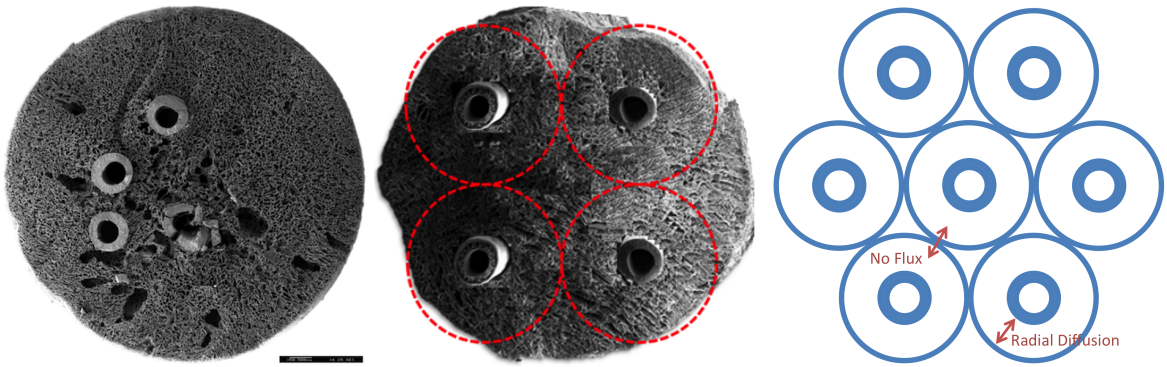

(a) Bioreactor (b) Idealised Hollow fibre Spacing (c) Krogh Cylinder Approximation

Figure 4: Bioreactor Cross Sections

mately $\varepsilon_{\mathrm{R,HF}} = 0.14$ so that any bioreactor must satisfy:

$$\varepsilon_{\mathrm{R,HF}} \cdot R_4^2 \geq N_{\mathrm{HF,PAN}}\, R_{2,\mathrm{PAN}}^2 + N_{\mathrm{HF,CRM}}\, R_{2,\mathrm{CRM}}^2 \tag{9}$$

Bioreactor geometry: Total volume in a single bioreactor available for growing cells:

$$\mathrm{Vol}_R = \pi\,(L - L_e)\,\left[R_4^2 - N_{\mathrm{HF,PAN}}\, R_{2,\mathrm{PAN}}^2 - N_{\mathrm{HF,CRM}}\, R_{2,\mathrm{CRM}}^2\right] \tag{10}$$

Krogh cylinder: Figures 4 and 5 show how the bioreactor is approximated using Krogh cylinders; Krogh cylinder dimensions are calculated for individual species because we assume each set of HF operates independently. Section 4.3 discusses permitted exchange in each HF type.

Krogh volume:

$$\mathrm{Vol}_{K,k} = \begin{cases} \frac{\pi\cdot(L-L_e)\cdot R_4^2}{N_{\mathrm{HF,PAN}}} & k = \mathrm{Glc,\ Lac} \\ \frac{\pi\cdot(L-L_e)\cdot R_4^2}{N_{\mathrm{HF,CRM}}+N_{\mathrm{HF,PAN}}} & k = \mathrm{O_2} \\ \frac{\pi\cdot(L-L_e)\cdot R_4^2}{N_{\mathrm{HF,CRM}}} & k = \mathrm{EPO,\ SCF} \end{cases} \tag{11}$$

Krogh radius:

$$R_{3,k} = \sqrt{\frac{\mathrm{Vol}_{K,k}}{\pi\,(L - L_e)}} \quad \forall\, k \tag{12}$$

Bioreactor parallelisation

$$\mathrm{Vol}_T = N_{\mathrm{R}}\ \mathrm{Vol}_R \tag{13}$$

The most critical set of substructures missing from the previous analysis (Equations 8 – 13) is the porous polyurethane (PU) scaffold mimicking the specialised 3D micro-environment struc-

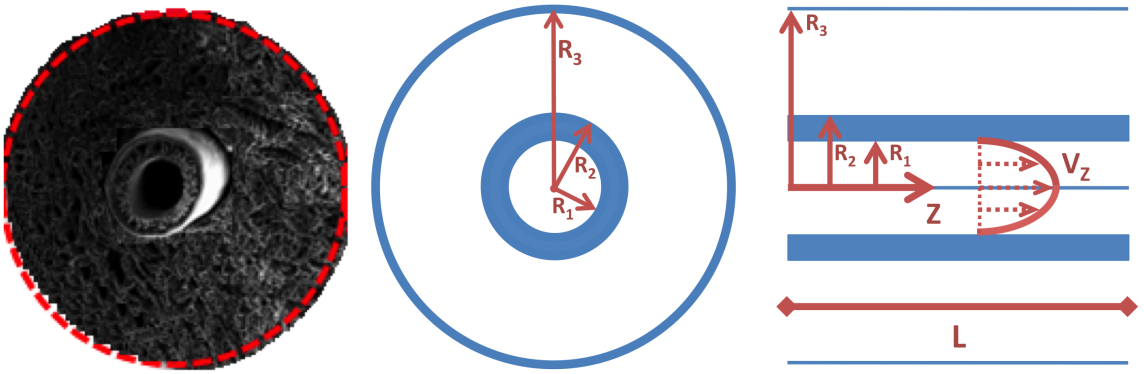

(a) Hollow fibre and Scaffold (b) Variable Definitions

Figure 5: Analysis of One Krogh Cylinder

ture of the bone marrow. The implicit assumption is that these micro-structures consistently exist in proportion to those present in Panoskaltsis et al. (2005).

5.3. Mass Transfer Equations

5.3.1. Shear Stress

A shear stress of 10 N/m^2 causes mild deformation of RBC; shear stress of 40 N/m^2 is enough to cause physiological damage by tearing endothelial cells away from the lining of the aorta; shear stress of 200 N/m^2 haemolyses RBC (Caro et al., 2012). To compare the shear stresses an RBC can handle with the shear stresses present in the bioreactor, we consider the maximum shear stress in a pipe operated with Poiseuille flow, $4 \cdot \mu \cdot U_Z / R_1$. Using $\mu = 691.38 \times 10^{-6}$ kg/m/s [NIST; water at 37 ^{o}C], $\hat{U_Z} = 8.8 \times 10^{-4}$ m/s, and $R_1 = 0.25$ mm, the shear stress is 2.4×10^{-3} N/m^2 and there is no danger that the cells will be damaged.

5.3.2. Entrance Effects

The density of blood ($\rho = 1.06 \cdot 10^3$ kg/m^3) is very similar to the density of water ($\rho = 1.00 \cdot 10^3$ kg/m^3), so we can assume that the fluid in the bioreactor lumen has a density very similar to 1. The dynamic viscosity of water at 37 ^{o}C is $\mu = 691.38 \times 10^{-6}$ kg/m/s [NIST], so the Reynolds number in the lumen is:

$$\mathrm{Re} = \frac{\rho \cdot U_Z \cdot 2 \cdot R_1}{\mu} = 7.2 \times 10^2 \frac{\mathrm{s}}{\mathrm{m}} \cdot U_Z \tag{14}$$

and the entrance length in the lumen, $L_e = 0.06 \cdot \mathrm{Re} \cdot L$ will be 5.8 mm for a bioreactor operated at the conditions used by Panoskaltsis et al. (2012) and Macedo (2011) and in general equal to:

$$L_e = 4.3 \times 10^1 \frac{\text{s}}{\text{m}} \cdot U_Z \cdot L\,; \tag{15}$$

the entry length has to be shaved off of the effective length of the bioreactor.

5.3.3. Krogh Approximation

All species $k \in \{\text{Glucose, Lactate, } O_2\text{, SCF, EPO}\}$ are bounded by the maximum $C_{k,\text{MAX}}$ and minimum $C_{k,\text{MIN}}$ concentrations given in Table 3:

$$C_{k,\text{MIN}} \leq C_{k,i}(r,z) \leq C_{k,\text{MAX}} \quad \forall\, i,k \tag{16}$$

Governing equations are taken from Jayaraman (1992) based on the Krogh (1919) model:

$$\begin{aligned}
&\text{R1; Lumen} && \frac{D_1}{r}\left(r\,\frac{\partial C_{k,1}(r,z)}{\partial r}\right) &&= U_z\left(1-\frac{r^2}{R_1^2}\right)\frac{\partial C_{k,1}(r,z)}{\partial z} && \forall\, k\\
&\text{R2; Membrane} && \frac{D_2}{r}\left(r\,\frac{\partial C_{k,2}(r,z)}{\partial r}\right) &&= 0 && \forall\, k\\
&\text{R3; Scaffold} && \frac{D_3}{r}\left(r\,\frac{\partial C_{k,3}(r,z)}{\partial r}\right) &&= \text{Rxn}_k && \forall\, k
\end{aligned} \tag{17}$$

Where the reaction term Rxn_k is described by the Michaelis Menten equation:

$$\text{Rxn}_k = \frac{V_k \cdot C_{k,3}}{K_{M,k} + C_{k,3}} \quad \forall\, k. \tag{18}$$

If $K_{M,k} \ll C_{k,3}$, then we can use the zero-order reaction limit $\text{Rxn}_k = V_k$; whereas if $K_{M,k} \gg C_{k,3}$, then we can use the first-order reaction limit $\text{Rxn}_k = V_k \cdot C_{k,3}/K_{M,k}$. We will use the zero-order approximation to simplify the analysis.

Equation Set (17) has the following boundary conditions:

$$
\begin{aligned}
&\text{R1; Lumen} \\
&\quad \text{Known inlet concentration:} \\
&\qquad C_{k,1}(r,z)\big|_{z=0} && = C_{k,\mathrm{IN}} && \forall\, k \\
&\quad \text{Known outlet concentration:} \\
&\qquad \textstyle\int_{r=0}^{R_1} C_{k,1}(r,z)\big|_{z=L}\, 2\,\pi\, r\, \mathrm{d}r && = C_{k,\mathrm{OUT}} && \forall\, k \\
&\quad \text{Radial symmetry:} \\
&\qquad \left.\frac{\partial C_{k,1}(r,z)}{\partial r}\right|_{r=0} && = 0 && \forall\, k \\
&\text{R2; Membrane} \\
&\quad \text{Flux across boundaries:} \\
&\qquad D_{k,1}\left.\frac{\partial C_{k,1}(r,z)}{\partial r}\right|_{r=R_1} && = D_{k,2}\left.\frac{\partial C_{k,2}(r,z)}{\partial r}\right|_{r=R_1} && \forall\, k \\
&\text{R3; Scaffold} \\
&\quad \text{Flux across boundaries:} \\
&\qquad D_{k,2}\left.\frac{\partial C_{k,2}(r,z)}{\partial r}\right|_{r=R_2} && = D_{k,3}\left.\frac{\partial C_{k,3}(r,z)}{\partial r}\right|_{r=R_2} && \forall\, k \\
&\quad \text{Symmetry at Krogh Cylinder boundaries:} \\
&\qquad D_{k,3}\left.\frac{\partial C_{k,3}(r,z)}{\partial r}\right|_{r=R_3} && = 0 && \forall\, k
\end{aligned}
\tag{19}
$$

Numerical solutions to the Krogh (1919) model are common (Kumar et al., 2004, 2008; Ma et al., 2007, 2012), but for integration into an optimisation model we would like to use either an analytical solution or an analytical function approximating a numerical solution.

For the conditions assumed in Table 1 (*i.e.*, zero-order reaction kinetics and parabolic laminar flow in the lumen), we can adopt the analytical solution of Piret and Cooney (1991):

$$C_{k,1}(z) = \left(R_2 - \frac{R_3^2}{R_2}\right) \cdot \left(\frac{\mathrm{N}_{HF} \cdot \mathrm{V}_k}{L \cdot U_Z}\right) \cdot z + \mathrm{C}_{k,\mathrm{IN}} \qquad \forall\, k \tag{20}$$

$$C_{k,2}(r,z) = \frac{V_k}{D_{k,3}}\ \left(R_3^2 - R_2^2\right)\ \left(\frac{11}{48} + \frac{1}{2\cdot\varepsilon_{HF}} \ln\frac{r}{R_1}\right) + C_{k,1}(z) \qquad \forall\, k \tag{21}$$

$$C_{k,3}(r,z) = \frac{V_k}{D_{k,3}}\ \left(\frac{R_3^2}{2}\ln\frac{r}{R_2} - \frac{r^2 - R_2^2}{4}\right) + C_{k,2}(R_2,z) \qquad \forall\, k \tag{22}$$

By Eq. (20), the bulk concentration of exiting species is:

$$C_{k,\mathrm{OUT}} = \left(R_2 - \frac{R_3^2}{R_2}\right) \cdot \left(\frac{\mathrm{N}_{HF} \cdot \mathrm{V}_k}{U_Z}\right) + \mathrm{C}_{k,\mathrm{IN}} \quad \forall\, k \tag{23}$$

Loss across hollow fibres is also due to Piret and Cooney (1991):

$$C_{k,\mathrm{LOSS}} = \frac{V_k}{D_{k,3}} \left(R_3^2 - R_2^2\right) \left(\frac{11}{48} + \frac{1}{2 \cdot \varepsilon_{HF}} \ln \frac{R_2}{R_1}\right) \quad \forall\, k \tag{24}$$

Given our assumption of Krogh's model, there are exactly two points that matter to our analysis: $(r = R_2, z = L_e)$, the entry length into the bioreactor, and $(r = R_3, z = L)$, the exit from the bioreactor. Because of our assumption of homogeneously distributed cells, the species concentrations at these two points must bound the concentrations in the remainder of the scaffold.

Important Point 1: Concentration at the bioreactor entrance, right near the lumen wall:

$$C_{k,2}(r = R_2, z = L_e) = C_{k,\mathrm{IN}} - C_{k,\mathrm{LOSS}} \quad \forall\, k \tag{25}$$

Important Point 2: Concentration at bioreactor exit, furthest relevant point from lumen:

$$C_{k,3}(r = R_3, z = L) = \frac{V_k}{D_{k,3}} \left(\frac{R_3^2}{2} \ln \frac{R_3}{R_2} - \frac{R_3^2 - R_2^2}{4}\right) + C_{k,\mathrm{OUT}} - C_{k,\mathrm{LOSS}} \quad \forall\, k \tag{26}$$

5.4. Bioreactor Initialisation

As shown in Table 5 of Section 4.4, there is an expected composition of mononuclear cells in UCB. The model selects inoculum cell density, but it cannot control cellular composition:

$$H_{E,0} = 0 \tag{27}$$

$$H_{G,0} = \frac{\hat{H}_{G,\mathrm{UCB}}}{\hat{H}_{Q,\mathrm{UCB}}} H_{Q,0} \tag{28}$$

$$H_{L,0} = \frac{\hat{H}_{L,\mathrm{UCB}}}{\hat{H}_{Q,\mathrm{UCB}}} H_{Q,0} \tag{29}$$

5.5. Cellular Kinetics: Growth, Proliferation, and Differentiation

The model for cellular growth, proliferation, and differentiation is derived from Ma et al. (2007, 2012) and Colijn and Mackey (2005). The adapted model of Ma et al. (2007, 2012) and Colijn and Mackey (2005), illustrated in Figure 2, uses delay differential equations to model cellular kinetics; we simplify our approach for the design problem by assuming that the bioreactor

operates at four discrete quasi-steady states. The proliferation rate $\beta(H_Q)$ is modelled as a Hill Function (Eq 34) and the entry into the erythroid (κ_E) and other leukocyte (κ_L) lineages is controlled using feedback functions (Eq 35 – 36). The death rates: γ_Q, γ_L, and γ_E are for each type of cell with respect to the times (τ_Q, τ_{LM}, τ_{LS}, τ_{EM}, τ_{ES}) that the cells require to proliferate and differentiate. There are many alternate models of erythropoiesis (Belair et al., 1995); the model proposed here could be easily swapped for another one.

Renewal of HSC, H_Q, and loss to differentiation (Colijn and Mackey, 2005; Ma et al., 2012):

$$\frac{dH_Q}{dt} = -\beta(H_Q)\, H_Q - (\kappa_E + \kappa_L + \kappa_G)\; H_Q + 2\, e^{-\gamma_S\, \tau_Q}\; \beta\left(H_Q(t-\tau_Q)\right)\; H_Q(t-\tau_Q) \tag{30}$$

Production of RBC, H_E (Colijn and Mackey, 2005; Ma et al., 2012):

$$\begin{aligned}\frac{dH_E}{dt} =& -(\gamma_E + \gamma_P)\, H_E \\ &+ A_E \left(\kappa_E(H_{E,\tau_{EM}})\; H_{Q,\tau_{EM}} - \underbrace{e^{-\gamma_E\; (\tau_{EM}+\tau_{ES})}\; \kappa_E(H_{E,\tau_{EM}+\tau_{ES}})\; H_{Q,\tau_{EM}+\tau_{ES}}}_{\text{Age related death}} \right)\end{aligned} \tag{31}$$

Production of lymphocytes, H_L (Colijn and Mackey, 2005; Ma et al., 2012):

$$\frac{dH_L}{dt} = -(\gamma_L + \gamma_P)\, H_L + A_L\; \kappa_L(H_{L,\tau_{LM}})\; H_{Q,\tau_{LM}} \tag{32}$$

Production of granulocytes and monocytes, H_G (Colijn and Mackey, 2005; Ma et al., 2012):

$$\begin{aligned}\frac{dH_G}{dt} =& -(\gamma_G + \gamma_P)\, H_G \\ &+ A_G \left(\kappa_G(H_{G,\tau_{GM}})\; H_{Q,\tau_{GM}} - \underbrace{e^{-\gamma_G\; \tau_{GS}}\; \kappa_G(H_{G,\tau_{GM}+\tau_{GS}})\; H_{Q,\tau_{GM}+\tau_{GS}}}_{\text{Age related death}} \right)\end{aligned} \tag{33}$$

where (Colijn and Mackey, 2005; Ma et al., 2012):

$$\beta(H_Q) = \frac{K_Q\; \theta^{c_Q}}{\theta^{c_Q} + Q^{c_Q}} \tag{34}$$

$$\kappa_E(H_E) = \frac{\overline{\kappa}_E}{1 + K_E\; E^{c_E}} \tag{35}$$

$$\kappa_L(H_L) = \frac{\overline{\kappa}_L \cdot \theta_2^{c_L}}{\theta_2^{c_L} + B^{c_L}} \tag{36}$$

$$\kappa_G(H_G) = \frac{\overline{\kappa}_G}{1 + K_G\; P^{c_G}} \tag{37}$$

Feeding Eqs. (30) – (37) into an optimisation algorithm is both computationally difficult and biologically irrelevant. This model of erythropoiesis has 26 uncertain parameters; effectively integrating it into a model of bioreactor operation requires simplifications. First, we argue that the age-related death terms in Eq. (31) & (33) are negligible. For RBC, time-to-senescence is ≈ 120 days (Colijn and Mackey, 2005) and the bioreactor only operates for 35 days. For granulocytes, the SCF and EPO added to the bioreactor encourages differentiation in the erythrocyte lineage and limits differentiation towards granulocytes. We also drop Eqs. (34) – (37); we have no way of differentiating the 12 parameters in those equations from one another once the erythropoiesis model is integrated into the bioreactor design model.

Discretising the 35-day bioreactor run into 5, week-long time periods, Eqs. (30) – (33) become:

$$\begin{aligned}
\frac{H_{Q,t}-H_{Q,t-1}}{\Delta t} &= -\left(\kappa_{E,t-1}+\kappa_{G,t-1}+\kappa_{L,t-1}\right)\cdot H_{Q,t-1} \\
&\quad +\left(2\cdot e^{-\gamma_S\cdot\tau_Q}-1\right)\cdot\beta_{Q,t-1}\cdot H_{Q,t-1} \qquad \forall t\in\{1,\ldots,5\} \qquad (38)\\
\frac{H_{E,t}-H_{E,t-1}}{\Delta t} &= -\left(\gamma_E+\gamma_{P,t}\right)\cdot H_{E,t-1}+A_E\cdot\kappa_{E,t-1}\cdot H_{Q,t-1} \qquad \forall t\in\{1,\ldots,5\} \qquad (39)\\
\frac{H_{L,t}-H_{L,t-1}}{\Delta t} &= -\left(\gamma_L+\gamma_{P,t}\right)\cdot H_{L,t-1}+A_L\cdot\kappa_{L,t-1}\cdot H_{Q,t-1} \qquad \forall t\in\{1,\ldots,5\} \qquad (40)\\
\frac{H_{G,t}-H_{G,t-1}}{\Delta t} &= -\left(\gamma_G+\gamma_{P,t}\right)\cdot H_{G,t-1}+A_G\cdot\kappa_{G,t-1}\cdot H_{Q,t-1} \qquad \forall t\in\{1,\ldots,5\} \qquad (41)
\end{aligned}$$

where $t=0$ is defined with respect to the inoculum conditions in Section 4.4 and the relevant decision variables from the objective function are $H_{h,0}$. The variables $\beta_{Q,t}$, $\kappa_{E,t}$, $\kappa_{G,t}$, $\kappa_{L,t}$ are restricted to the ranges in Table B.9. Observe that this first-order forward Euler discretisation may be unstable with respect to the Ma et al. (2007, 2012) model but that it is an acceptable model for capturing erythropoiesis trends until we have more extensive experimental data.

5.5.1. Species Consumption and Production

The species consumption and production equations in this section connect the Section 5.3 mass transfer equations with the Section 5.5 cellular kinetics. Because we are assuming zero order reactions, cells can only exist in locations falling in the acceptable species concentration ranges (Table 3). These reaction rates V_k and $V_{O_2,h}$ limit the average cellular concentrations $H_{h,t}$ to the number of cells that the bioreactor mass transfer rates can support.

Reaction Rate of Glucose and Lactate: Assumed constant; see Section 4.6.

Reaction Rate of Oxygen: Assume, as in Section 4.6, that cells in the bone marrow haematopoi-

etic compartment consume oxygen consistent with Table 7 (Chow et al., 2001):

$$V_{O_2} = V_{O_2,Q} \cdot H_{Q,t} + V_{O_2,L} \cdot H_{L,t} + V_{O_2,E} \cdot H_{E,t} + V_{O_2,G} \cdot H_{G,t} \quad \forall t \in \{1, \ldots, 5\} \tag{42}$$

Reaction Rate of EPO: Our quantitative estimate that we need 2.1 EPO molecules per RBC produced is defined in Section 4.6. Assuming that even cells dying during differentiation need EPO, the reaction rate is $V_{\text{EPO}}\left[\text{U}/\text{m}^3/\text{day}\right]$:

$$\begin{aligned} V_{\text{EPO}} &= A_E \cdot \kappa_E \cdot H_{Q,t} \cdot \frac{2.1 \text{ EPO}}{\text{RBC}} \cdot \frac{1 \text{ mol EPO}}{6.022 \times 10^{23} \text{ EPO}} \cdot \frac{3.4 \times 10^7 \text{ mg}}{1 \text{ mol EPO}} \cdot \frac{1.29 \times 10^5 \text{ U}}{1 \text{ mg}} \\ &= 1.8 \times 10^{-5} \cdot \kappa_{E,t} \cdot H_{Q,t} \qquad \forall t \in \{1, \ldots, 5\} \end{aligned} \tag{43}$$

Note that Eq. (43) indicates that losses due to EPO reaction will be much less than losses due to half-life decay.

Reaction Rate of SCF: Assumed constant and negligble; see Section 4.6.

EPO and SCF: Half-Life Based Replenishment Rate

From the analysis in Section 4.2, the half-life of EPO and SCF is 72 and 48 hours, respectively. Then if we run the culture for 35 days and we topped up the EPO and SCF every day then we would have to add:

$$\sum_{d=0}^{35} C_0 \left(1 - 2^{-1/t_{1/2}}\right) = \begin{cases} \sum_{d=0}^{35} C_{0,\text{EPO}} \left(1 - 2^{-1/3}\right) = 7.22\, C_{0,\text{EPO}} \\ \sum_{d=0}^{35} C_{0,\text{SCF}} \left(1 - 2^{-1/2}\right) = 10.2\, C_{0,\text{SCF}} \end{cases} \tag{44}$$

over the course of the culture. In the limit as the additions of EPO and SCF become more frequent, we will have to add ≈ 8.09 and ≈ 12.1 times the original value of EPO and SCF, respectively, to stay constant:

$$\tau_k \cdot C_{0,k} = \lim_{n \to \infty} 2^n \frac{T}{t_{1/2}} \left(1 - 2^{-1/2^n}\right) \cdot C_{0,k} \approx \begin{cases} 8.09\, C_{0,\text{EPO}} \\ 12.1\, C_{0,\text{SCF}} \end{cases} \tag{45}$$

We require that SCF be used in weeks 1 – 2 of the culture and EPO be used in weeks 2 – 5; SCF affects early-stage HSC proliferation and EPO is related to late-stage differentiation.

5.6. *Production Requirements*

The total concentration of haematopoietic cells $H_{\text{Cells},t}$ in the bioreactor may not exceed the bone marrow density (Peng and Palsson, 1996):

$$H_{\text{Cells},t} = H_{Q,t} + H_{E,t} + H_{L,t} + H_{G,t} \leq H_{\text{MAX}} \; \forall t \in \{1, \ldots, 5\}, \tag{46}$$

(Macedo, 2011, p. 177) showed that the average cellular flux across the ceramic hollow fibre was $\hat{J}_{\text{Cells}} = 5.76 \pm 2.25 \times 10^5$ cells / mm^2 / day when the concentration gradient across the membrane was $\Delta\hat{H}_{\text{Cells}} = 1.00 \times 10^6$ cells / mm^3. Observe from capillary theory that the flux across a filter is directly proportional to the concentration gradient (Caro et al., 2012); we assume that the cellular concentration in the lumen is negligible. Further, HSC $H_{Q,t}$ are assumed to *not* diffuse through the membrane because, due to their lower oxygen consumption, they are typically further away from the vasculature (Simsek et al., 2010).

The total surface area of available membrane in a single bioreactor is: $\pi \cdot N_{\text{HF,CRM}} \cdot R_{2,\text{CRM}} \cdot L$, so the production rate of cells out of a single bioreactor each day is:

$$\gamma_{P,t} = \frac{\hat{J}_{\text{Cells}}}{\Delta\hat{H}_{\text{Cells}}} \cdot \frac{\pi \cdot N_{\text{HF,CRM}} \cdot R_{2,\text{CRM}} \cdot L}{\text{Vol}_R} \; \forall t \in \{1, \ldots, 5\} \tag{47}$$

Eq. (48) constrains the system to produce at least one unit (Unit_{RBC}) of red blood cells in the total volume Vol_T over D days of processing time; $\gamma_{P,t}$ is the production rate of exiting $H_{E,t}$.

$$\sum_t \gamma_{P,t} \; \text{Vol}_T \; D_t \; \frac{H_{E,t} + H_{E,t-1}}{2} \geq \text{Unit}_{\text{RBC}} \tag{48}$$

As an order of magnitude analysis, consider the bioreactor of Panoskaltsis et al. (2012) consisting entirely of erythrocytes at maximum BM cell density; $\text{N}_R \approx 250$ bioreactors would be necessary to satisfy the Eq. (48) production requirement. The optimization model may try to provide better RBC transport by increasing the number of ceramic HF and the reactor length.

6. Solving the Model: Results and Discussion

The model developed in Sections 4 and 5 was implemented in GAMS 24.1. For clarity, the model is repeated in Appendix A and all relevant symbols are defined in Appendix B. The fully-implemented model has 261 variables (2 integer) and 205 equations. We solved the model to global optimality using the MINLP solver ANTIGONE 1.1 (Misener and Floudas, 2013a,b); ANTIGONE 1.1 is solver software implementing branch-and-cut deterministic global optimisation for MINLP. ANTIGONE 1.1 reformulates the problem to: 186 variables; 184 equations;

185 bilinear terms; 3 logarithmic terms; 50 reformulation-linearization technique equations. ANTIGONE 1.1 consistently solves this problem to a 10% duality gap within 300 CPU s.

Solving to deterministic global optimality ensures finding the best solution to the nominal optimisation problem. Furthermore, ANTIGONE 1.1 achieves not only good feasible solutions (primal bound) but also derives information as to how good the solution could possibly be (dual bound) and thereby rigorously characterises the solution. But both the parameters and the underlying model itself is uncertain (Misener et al., 2014), so we are only solving to an optimality gap of 10%; a tight duality gap is meaningless for these uncertain parameters. To better characterise the implications of the global optimisation procedure, we also conduct *what-if* scenarios (§6.2) and sensitivity analyses (§6.3).

Effectively characterising the *what-if* scenarios and sensitivities requires that ANTIGONE 1.1 regularly solve the model and parameter variants quickly. The key for solving this model quickly is careful scaling of all relevant variables and parameters; observe that the text of this manuscript has described both very small numbers (*e.g.*, O_2 consumption on the order of 10^{-15} mol / cell / day) and very large numbers (*e.g.*, a unit of blood consists of 10^{12} cells). The scaled model entered into GAMS is mathematically equivalent to the one presented in this paper.

6.1. Characteristics of the Optimal Solution

The global minimum is within 10% of US $ 277 ($N_R = 339$; US $ 0.82 / reactor). Observe that $N_R = 339$ is within the expected values calculated via order of magnitude analysis in Sections 4.5 & 5.6. The price per reactor is driven by half-life decay of EPO (US $ 0.298) and SCF (US $ 0.512); the growth factor reaction costs are negligible and the start-up costs are less than US $ 0.01 / reactor. Small start-up costs compared to operating costs are expected (Timmins and Nielsen, 2009); the only reason we include initialization costs in Eq. (7) is that otherwise the optimization model will drive the inoculum to have as many HSC as it needs to produce RBC.

Half-life decay of EPO and SCF are the most expensive component of bioreactor operation and we require $\text{Vol}_{\text{Recyc}} = 10^5$ mm^3 = 100 mL recycle volume per reactor, so the optimization model consistently maximises the allowable bioreactor length by distributing 20 HF into a bioreactor of length 200 mm (the physical limit of both variables). The optimisation objective is manufacturing 1 unit RBC at minimum cost, so the optimisation model pushes to incorporate as many ceramic hollow fibres as possible because only the ceramic membranes are capable of delivering RBC out of the bioreactor. In the nominal optimal solution there are 11 CRM and 9 PAN HF; this satisfies the limiting transport need to supply glucose with the remaining HF devoted to nutrient transport. The suggested 5.3 mm reactor radius is the smallest possible permitted by Eq. (9) with 20 HF; the narrow width of the bioreactor is to increase mass transfer

into the scaffold bulk.

The optimisation model also consistently pushes the lumen flow rate as high as it possibly can; this is to increase mass transfer within the reactor. Because the bioreactor is oxygen-limited (we cannot physically pack the bioreactor with fibres as tightly as the BM is packed with blood vessels), the optimization model recommends tailoring inoculum density and growth such that the maximum cell density is 1.86×10^8 cells / mL (less than half the physiological 5.0×10^8 cells / mL). Based on mathematical analysis of the nominal superstructure solution, we make the following design and operation recommendations:

- Hollow fibres should be able to **handle higher flow rates** to permit better mass transfer. Section 5.3.1 shows that the flowrate would have to increase by orders of magnitude to put the cells in danger of haemolysis; the hollow fibres are limiting the possibility of a higher flowrate. Section 5.3.2 shows that the flow should stay laminar until approximately 20 times the current flow rate.
- Use as **many hollow fibres as reasonably possible**; the limit is physical.
- Use the minimum number of PAN hollow fibres; the rest of the bioreactor should be **crammed with ceramic hollow fibres**. The purpose of the PAN hollow fibres is to fulfill the required nutrient transfer and waste clearance, but the ceramic hollow fibres are the ones that permit RBC crossing.
- Ceramic hollow fibres should be designed to be **more permeable to RBC**.
- Use as **long and narrow** a bioreactor as reasonably possible. The suggested long length comes from the penalty per bioreactor on recycle volume; a design choice reducing the recycle reservoir volume would allow us to equivalently shorten the bioreactor. Experimental experience suggests that hollow fibres in a shorter bioreactor are less likely to bend or break; the cost of malfunctioning bioreactors is not considered in this paper.

Observe that the global minimum for the bioreactor superstructure is US $ 277 / unit RBC in comparison to US $ 8330 as calculated by Timmins and Nielsen (2009) for the procedure of Giarratana et al. (2005); the bioreactor design of Panoskaltsis et al. (2012) is therefore competitive to a typical unit of rare blood (US $ 1150 – 3025). We do *not* claim that the bioreactor is competitive with mainstream transfusion (US $ 225.42 / unit) because the proposed mathematical model neglects the prices of: (1) nutrients; (2) bioreactor materials and fabrication; (3) operator time; (4) product transportation and storage.

6.2. What-If *Scenario Analysis*

The nominal superstructure design of the bioreactor is interesting in that it indicates the potential for the bioreactor of Panoskaltsis et al. (2012) to compete on the open market against rare blood transfusion. But it is also interesting to vary operating conditions for parameters that will qualitatively affect RBC production but lack mathematical correlations; results of this analysis are illustrated in Figure 6. Our nominal solution of US $ 277 assumes that the maximum allowable concentrations of glucose and O_2 are 25 mM and 20%, respectively; these correspond to the concentrations in the medium IMDM and operation at atmospheric conditions. But it may be beneficial to operate the bioreactor at physiological BM levels of glucose (maximum: 5.5 mM) and oxygen (maximum: 6%). As Figure 6 shows, changing the maximum allowable concentrations in the bioreactor alters the total price and the number of ceramic hollow fibres. The optimisation model still selects the same bioreactor dimensions (because these are largely dependent on the price of EPO and SCF) and still maximises the number of hollow fibres in the reactor ($N_{\mathrm{HF}} = 20$) for better mass transfer, but: (1) moving towards physiological conditions is more expensive because mass transfer to the scaffold bulk is more difficult; and (2) see in Figure 6 that the model always chooses to add as many ceramic hollow fibres as possible while still ensuring sufficient mass transfer of nutrients and metabolites.

6.3. *Parameter Sensitivity Analysis*

Because the parameters describing the bioreactor are uncertain, we performed a single-variable sensitivity study varying 29 uncertain parameters in Table B.9. We allowed parameters with known error bars to vary within their expected uncertainty levels; the remaining parameters were allowed to take values 50% (L1), 90% (L2), 110% (U1), and 150% (U2) of their nominal values. Of the 29 parameters, 11 induced the global optimum to vary by 10% or more; rank ordered with $\hat{J}_{\mathrm{Cells}}$ affecting the most change, they are:

$\hat{J}_{\mathrm{Cells}}$	Cellular flux across ceramic HF
$t_{1/2,\mathrm{SCF}}$	SCF growth factor half-life
p_{SCF}	Price of species SCF
A_E	Amplification parameter for RBC differentiation
$\mathrm{V}_{\mathrm{O_2,Gran}}$	Rxn rate of O_2 with cell type Gran in the scaffold
$t_{1/2,\mathrm{EPO}}$	EPO growth factor half-life
$\varepsilon_{\mathrm{HF}}$	Porosity of hollow fibre
p_{EPO}	Price of species EPO
$\mathrm{V}_{\mathrm{Glc}}$	Maximum rxn rate of species Glc in the scaffold
$\mathrm{V}_{\mathrm{O_2,HSC}}$	Rxn rate of O_2 with cell type HSC in the scaffold
A_G	Amplification parameter for Gran differentiation

Figure 7 diagramms the impact of these 11 parameters on the global optimum. The uncertainty in the cellular flux across ceramic HF $\hat{J}_{\text{Cells}}$ induces the most variability; this is inline with our observations in Section 6.1 that the bioreactor is always pushing to have as many of the RBC-harvesting ceramic hollow fibers as possible; it makes sense that impeding the movement of RBC through those HF makes producing a unit of blood more expensive.

Recall here that the missing step is to incorporate complete model uncertainty as we did in Misener et al. (2014); we are excluding uncertainty analysis in this manuscript due to space constraints. Sources of model uncertainty include: (1) species reaction rate; (2) cellular proliferation and differentiation rate; (3) exit rate of mature cells from the bioreactor.

The final contribution of this manuscript is to note the generalisation of our work to bioprocess optimisation; we have used the intellectual tools of process systems engineering to integrate bioreactor design and operation. Combining experimental data with previously-proposed mathematical models of mass transfer and cell kinetics has allowed us to develop an optimisation problem that will guide further development of the bioreactor.

7. Conclusions

This paper develops and optimises an integrated design and operation model of an RBC-producing bioreactor designed by Panoskaltsis et al. (2012). The mathematical novelty of our approach stems from: explicitly considering bioreactor design and incorporating a mathematical model of haematopoiesis into the optimisation problem. The engineering contribution is to show how this superstructure design strategy can generally impact bioprocess optimisation. The industrial contribution is to show, for the first time, the potential for *ex vivo* red blood cell production to compete openly against the transfusion market for rare blood. We discuss the potential of global superstructure design not only on this individual bioreactor but also more generally on bioprocess optimisation.

Acknowledgements:

This work is supported by: a Royal Academy of Engineering Research Fellowship to R.M; ERC-BioBlood (no. 340719); the Richard Thomas Leukaemia Research Fund.

8. Bibliography

J. W. Adamson. The relationship of erythropoietin and iron-metabolism to red-blood-cell production in humans. *Seminars in Oncology*, 21(2, 3):9–15, 1994.

J. R. Banga, R. Irizarry-Rivera, and W. D. Seider. Stochastic optimization for optimal and model-predictive control. *Comput. Chem. Eng.*, 22(4-5):603–612, 1998.

J. R. Banga, E. Balsa-Canto, C. G. Moles, and A. A. Alonso. Dynamic optimization of bioprocesses: Efficient and robust numerical strategies. *J. Biotechnol.*, 117(4):407–419, 2005.

C. Basford, N. Forraz, and C. McGuckin. Optimized multiparametric immunophenotyping of umbilical cord blood cells by flow cytometry. *Nat. Protoc.*, 5(7):1337–1346, 2010.

V. Becker, M. Schilling, J. Bachmann, U. Baumann, A. Raue, T. Maiwald, J. Timmer, and U. Klingmüller. Covering a broad dynamic range: Information processing at the erythropoietin receptor. *Science*, 328(5984):1404–1408, 2010.

J. Belair, M. C. Mackey, and J. M. Mahaffy. Age-structured and 2-delay models for erythropoiesis. *Mathematical Biosciences*, 128(1-2):317–346, 1995.

E. Beutler, M. A. Lichtman, B. S. Coller, T. J. Kipps, and U. Seligsohn. *Williams Hematology*. McGraw-Hill, Medical Publishing Division, 6 edition, 2001. ISBN 0-07-070397-3.

D. Boehm, W. G. Murphy, and M. Al-Rubeai. The effect of mild agitation on in vitro erythroid development. *J. Immunol. Methods*, 360(1-2):20–29, 2010.

D. A. Brindley, B. C. Reeve, W. A. Sahlman, G. A. Bonfiglio, N. L. Davie, E. J. Culme-Seymour, and C. Mason. The impact of market volatility on the cell therapy industry. *Cell Stem Cell*, 9(5):397 – 401, 2011.

J. D. Brotherton and P. C. Chau. Modeling of axial-flow hollow fiber cell culture bioreactors. *Biotechnol. Progr.*, 12(5):575–590, 1996.

V. C. Broudy. Stem cell factor and hematopoiesis. *Blood*, 90(4):1345–1364, 1997.

V. C. Broudy, F. O. Smith, N. Lin, K. M. Zsebo, J. Egrie, and I. D. Bernstein. Blasts from patients with acute myelogenous leukemia express functional receptors for stem cell factor. *Blood*, 80(1):60–67, 1992.

G. J. M. Cabrita, B. S. Ferreira, C. L. da Silva, R. Goncalves, G. Almeida-Porada, and J. M. S. Cabral. Hematopoietic stem cells: from the bone to the bioreactor. *Trends in Biotechnology*, 21(5):233–240, 2003.

C. G. Caro, T. J. Pedley, R. C. Schroter, and W. A. Seed. *The Mechanics of the Circulation*. Cambridge University Press, 2 edition, 2012.

D. C. Chow, L. A. Wenning, W. M. Miller, and E. T. Papoutsakis. Modeling pO(2) distributions in the bone marrow hematopoietic compartment. I. Krogh's model. *Biophys. J.*, 81(2):675–684, 2001.

T. J. Chresand, R. J. Gillies, and B. E. Dale. Optimum fiber spacing in a hollow fiber bioreactor. *Biotechnol. Bioeng.*, 32(8):983–992, 1988.

C. Colijn and M. C. Mackey. A mathematical model of hematopoiesis - I. Periodic chronic myelogenous leukemia. *Journal of Theoretical Biology*, 237(2):117–132, 2005.

E. Curcio, L. De Bartolo, G. Barbieri, M. Rende, L. Giorno, S. Morelli, and E. Drioli. Diffusive and convective transport through hollow fiber membranes for liver cell culture. *J. Biotechnol.*, 117(3):309–321, 2005.

A. J. Davidson, M. J. Ellis, and J. B. Chaudhuri. A theoretical method to improve and optimize the design of bioartificial livers. *Biotechnol. Bioeng.*, 106(6):980–988, 2010.

M. R. Doran, I. A. Aird, F. Marturana, N. Timmins, K. Atkinson, and L. K. Nielsen. Bioreactor for blood product production. *Cell Transplantation*, 21(6):1235–1244, 2012.

M. Drouet, F. Mourcin, N. Grenier, V. Leroux, J. Denis, J. F. Mayol, P. Thullier, J. J. Lataillade, and F. Herodin. Single administration of stem cell factor, FLT-3 ligand, megakaryocyte growth and development factor, and interleukin-3 in combination soon after irradiation prevents nonhuman primates from myelosuppression: long-term follow-up of hematopoiesis. *Blood*, 103(3):878–885, 2004.

A. Dutta and A. S. Popel. A theoretical-analysis of intracellular oxygen diffusion. *Journal of Theoretical Biology*, 176(4):433–445, 1995.

K. U. Eckardt, U. Boutellier, A. Kurtz, M. Schopen, E. A. Koller, and C. Bauer. Rate of erythropoietin formation in humans in response to acute hypobaric hypoxia. *J Applied Physiology*, 66(4):1785–1788, 1989.

S. Elliott, E. Pham, and I. C. Macdougall. Erythropoietins: A common mechanism of action. *Experimental Hematology*, 36(12):1573–1584, 2008.

S. J. England, K. E. McGrath, J. M. Frame, and J. Palis. Immature erythroblasts with extensive ex vivo self-renewal capacity emerge from the early mammalian fetus. *Blood*, 117(9):2708–2717, 2011.

A. Ganser, B. Völkers, P. Scigalla, and D. Hoelzer. Effect of human recombinant erythropoietin on human hemopoietic progenitor cells in vitro. *Klinische Wochenschrift*, 66(6):236–240, 1988.

M.-C. Giarratana, L. Kobari, H. Lapillonne D. Chalmers, L. Kiger, T. Cynober, M. C. Marden, H. Wajcman, and L. Douay. Ex vivo generation of fully mature human red blood cells from hematopoietic stem cells. *Nat Biotech*, 23(1):69–74, 2005.

M.-C. Giarratana, H. Rouard, A. Dumont, L. Kiger, I. Safeukui, P.-Y. Le Pennec, S. Francois, G. Trugnan, T. Peyrard, T. Marie, S. Jolly, N. Hebert, C. Mazurier, N. Mario, L. Harmand, H. Lapillonne, J.-Y. Devaux, and L. Douay. Proof of principle for transfusion of in vitro-generated red blood cells. *Blood*, 118(19):5071–5079, 2011.

S. M. Hattangadi, P. Wong, L. Zhang, J. Flygare, and H. F. Lodish. From stem cell to red cell: regulation of erythropoiesis at multiple levels by multiple proteins, rnas, and chromatin modifications. *Blood*, 118(24):6258–6268, 2011.

M. G. V. Heiden, L. C. Cantley, and C. B. Thompson. Understanding the Warburg effect: The metabolic requirements of cell proliferation. *Science*, 324(5930):1029–1033, 2009.

C. Hindorf, G. Glatting, C. Chiesa, O. Linden, and G. Flux. EANM dosimetry committee guidelines for bone marrow and whole-body dosimetry. *Eur. J. Nucl. Med. Mol. Imaging*, 37 (6):1238–1250, 2010.

G. J. Housler, T. Miki, E. Schmelzer, C. Pekor, X. Zhang, L. Kang, V. Voskinarian-Berse, S. Abbot, K. Zeilinger, and J. C. Gerlach. Compartmental hollow fiber capillary membrane-based bioreactor technology for in vitro studies on red blood cell lineage direction of hematopoietic stem cells. *Tissue Eng. Part C-Methods*, 18(2):133–142, 2012.

V. K. Jayaraman. The solution of hollow fiber bioreactor design equations. *Biotechnol. Progr.*, 8(5):462–464, 1992.

K. Kaushansky. Mechanisms of disease: Lineage-specific hematopoietic growth factors. *New England Journal of Medicine*, 354(19):2034–2045, 2006.

M. R. King. Biomedical applications of microchannel flows. In S. Kandlikar, S. Garimella, D. Li, S. Colin, and M. R. King, editors, *Heat Transfer and Fluid Flow in Minichannels and Microchannels*, pages 409–442. Elsevier Science, New York, 2005.

S. Kishimoto, F. Oonuma, S. Nakamura, H. Hattori, S.-I. Nakamura, Y. Mori, Y. Tanaka, Y. Harada, M. Tagawa, and M. Ishihara. Immobilization, stabilization, and activation of human stem cell factor (SCF) on fragmin/protamine microparticle (F/P MP)- coated plates. *J. Biomedical Materials Res. Part B-Applied Biomaterials*, 92B(1):32–39, 2010.

M. R. O. B. Koller, M. S. Bradley, and B. O. Palsson. Growth-factor consumption and production in perfusion cultures of human bone-marrow correlate with specific cell production. *Experimental Hematology*, 23(12):1275–1283, 1995.

F. Kreuzer. Oxygen-supply to tissues - the Krogh model and its assumptions. *Experientia*, 38 (12):1415–1426, 1982.

A. Krogh. The number and distribution of capillaries in muscles with calculations of the oxygen pressure head necessary for supplying the tissue. *J. Physiol.*, 52:409–415, 1919.

R. Kumar, F. Stepanek, and A. Mantalaris. An oxygen transport model for human bone marrow microcirculation. *Food and Bioproducts Processing*, 82(C2):105–116, 2004.

R. Kumar, N. Panoskaltsis, F. Stepanek, and A. Mantalaris. Coupled oxygen-carbon dioxide transport model for the human bone marrow. *Food and Bioproducts Processing*, 86(C3): 211–219, 2008.

M. Labecki, B. D. Bowen, and J. M. Piret. Two-dimensional analysis of protein transport in the extracapillary space of hollow-fibre bioreactors. *Chemical Engineering Science*, 51(17): 4197–4213, 1996.

K. E. Langley, L. G. Bennett, J. Wypych, S. A. Yancik, X. D. Liu, K. R. Westcott, D. G. Chang, K. A. Smith, and K. M. Zsebo. Soluble stem-cell factor in human serum. *Blood*, 81 (3):656–660, 1993.

R. Lawes. Nhs blood and transplant commercial review, 2011. Report 16588, https://www.gov.uk/government/uploads/system/uploads/attachment_data/file/215390/dh_130563.pdf, Accessed 28 Jan 2014.

J. Lennartsson and L. Ronnstrand. Stem cell factor receptor/c-KIT: From basic science to clinical implications. *Physiological Reviews*, 92(4):1619–1649, 2012.

C. Lobato da Silva, R. Goncalves, F. Lemos, M. A. N. D. A. Lemos, E. D. Zanjani, G Almeida-Porada., and J. M. S. Cabral. Modelling of ex vivo expansion/maintenance of hematopoietic stem cells. *Bioprocess and Biosystems Engineering*, 25(6):365–369, 2003.

H. Lodish, J. Flygare, and S. Chou. From stem cell to erythroblast: Regulation of red cell production at multiple levels by multiple hormones. *IUBMB LIFE*, 62(7):492–496, 2010.

S.-J. Lu, Q. Feng, J. S. Park, L. Vida, B.-S. Lee, M. Strausbauch, P. J. Wettstein, G. R. Honig, and R. Lanza. Biologic properties and enucleation of red blood cells from human embryonic stem cells. *Blood*, 112(12):4475–4484, 2008.

C. Y. J. Ma, R. Kumar, X. Y. Xu, and A. Mantalaris. A combined fluid dynamics, mass transport and cell growth model for a three-dimensional perfused biorector for tissue engineering of haematopoietic cells. *Biochem. Eng. J.*, 35(1):1–11, 2007.

C. Y. J. Ma, N. Panoskaltsis, R. Kumar, X. Y. Xu, and A. Mantalaris. Simulation of ex vivo bone marrow culture: Application to chronic myeloid leukaemia growth model. *Biochem. Eng. J.*, 61:66–77, 2012.

H. M. Macedo. *A Novel 3D Dual Hollow Fibre Bioreactor for the Production of Human Red Blood Cells*. PhD thesis, Imperial College London, 2011.

J. M. Mahaffy, J. Belair, and M. C. Mackey. Hematopoietic model with moving boundary condition and state dependent delay: Applications in erythropoiesis. *J. Theor. Biol.*, 190(2): 135–146, 1998.

A. Mantalaris, P. Keng, P. Bourne, A. Y. C. Chang, and J. H. D. Wu. Engineering a human bone marrow model: A case study on ex vivo erythropoiesis. *Biotechnol. Progr.*, 14(1):126–133, 1998.

C. Mason, D. A Brindley, and E. J Culme-Seymour. Cell therapy industry: billion dollar global business with unlimited potential. *Regen Med*, 6(3):265–272, 2011.

J. C. Maxwell. *Treatise on Electricity and Magnetism*, volume 1. Clarendon Press, Oxford, 2 edition, 1881.

G. M. Meny, C. Flickinger, and C. Marcucci. The American Rare Donor Program. *Journal of Critical Care*, 28(1), 2013.

D. Metcalf. Hematopoietic cytokines. *Blood*, 111(2):485–491, 2008.

K. Miharada, T. Hiroyama, K. Sudo, T. Nagasawa, and Y. Nakamura. Efficient enucleation of erythroblasts differentiated in vitro from hematopoietic stem and progenitor cells. *Nat Biotech*, 24(10):1255–1256, 2006.

R. Misener and C. A. Floudas. ANTIGONE: Algorithms for coNTinuous / Integer Global Optimization of Nonlinear Equations. *J. Glob. Optim.*, 59(2-3):503–526, 2013a.

R. Misener and C. A. Floudas. GloMIQO: Global Mixed-Integer Quadratic Optimizer. *J. Glob. Optim.*, 57:3–30, 2013b.

R. Misener, J. Chin, M. Lai, M. Fuentes-Garí, E. Velliou, N. Panoskaltsis, E. N. Pistikopoulos, and A. Mantalaris. Robust superstructure optimisation of a bioreactor that produces red blood cells. In P. Mizsey J. Klemes, F. Friedler, editor, *24th European Symposium on Computer Aided Process Engineering*, volume 33 of *Computer-Aided Chemical Engineering*, pages 91–96, 2014.

T. Mortera-Blanco, A. Mantalaris, A. Bismarck, N. Aqel, and N. Panoskaltsis. Long-term cytokine-free expansion of cord blood mononuclear cells in three-dimensional scaffolds. *Biomaterials*, 32(35):9263 – 9270, 2011.

B. C. Mulukutla, S. Khan, A. Lange, and W.-S. Hu. Glucose metabolism in mammalian cell culture: new insights for tweaking vintage pathways. *Trends Biotechnol.*, 28(9):476–484, 2010.

NHS. Blood and transplant: Umbilical cord blood price, 2013. Paid by Biological Systems Engineering Laboratory.

E. N. Olivier, C. Qiu, M. Velho, R. E. Hirsch, and E. E. Bouhassira. Large-scale production of embryonic red blood cells from human embryonic stem cells. *Experimental Hematology*, 34(12):1635 – 1642, 2006.

S. S. Ozturk, J. C. Thrift, J. D. Blackie, and D. Naveh. Real-time monitoring and control of glucose and lactate concentrations in a mammalian cell perfusion reactor. *Biotechnol. Bioeng.*, 53(4):372–378, 1997.

N. Panoskaltsis, A. Mantalaris, and J. H. D. Wu. Engineering a mimicry of bone marrow tissue ex vivo. *J. Bioscience Bioengineering*, 100(1):28–35, 2005.

N. Panoskaltsis, H. M. M. Macedo, M. T. M. Blanco, A. Mantalaris, and A. G. Livingston. 3-dimensional hollow fibre bioreactor systems for the maintenance, expansion, differentiation and harvesting of human stem cells and their progeny, 2012. Patent. WO 2012/069841 A1.

B. Panzenbock, P. Bartunek, M. Y. Mapara, and M. Zenke. Growth and differentiation of human stem cell factor erythropoietin-dependent erythroid progenitor cells in vitro. *Blood*, 92(10):3658–3668, 1998.

C. A. Peng and B. O. Palsson. Determination of specific oxygen uptake rates in human hematopoietic cultures and implications for bioreactor design. *Annals of Biomedical Engineering*, 24(3):373–381, 1996.

J. C. Pichardo, A. A. Trindade, J. M. Brindle, and W. E. Bolch. Method for estimating skeletal spongiosa volume and active marrow mass in the adult male and adult female. *J. Nucl. Med.*, 48(11):1880–1888, 2007.

J. M. Piret and C. L. Cooney. Model of oxygen-transport limitations in hollow fiber bioreactors. *Biotechnol. Bioeng.*, 37(1):80–92, 1991.

D. A. Rew and G. D. Wilson. Cell production rates in human tissues and tumours and their significance. Part II: Clinical data. *Eur. J. Surg. Oncol.*, 26(4):405–417, 2000.

A. C. F. Ribeiro, V. M. M. Lobo, D. G. Leaist, J. J. S. Natividade, L. P. Verissimo, M. C. F. Barros, and A. M. T. D. P. V. Cabral. Binary diffusion coefficients for aqueous solutions of lactic acid. *J. Solution Chem.*, 34(9):1009–1016, 2005.

A. Riccardi, M. Danova, G. Wilson, G. Ucci, P. Dormer, G. Mazzini, S. Brugnatelli, M. Girino, N. J. McNally, and E. Ascari. Cell-kinetics in human malignancies studied with in vivo administration of bromodeoxyuridine and flow-cytometry. *Cancer Res.*, 48(21):6238–6245, 1988.

G. F. Rousseau, M.-C. Giarratana, and L. Douay. Large-scale production of red blood cells from stem cells: what are the technical challenges ahead? *Biotechnol. J.*, 9(1):28–38, 2014.

K. E. Schlageter, P. Molnar, G. D. Lapin, and D. R. Groothuis. Microvessel organization and structure in experimental brain tumors: Microvessel populations with distinctive structural and functional properties. *Microvasc. Res.*, 58(3):312–328, 1999.

L. Sensebe, B. T. Mortensen, P. Fixe, P. Herve, and P. Charbord. Cytokines active on granulomonopoiesis: Release and consumption by human marrow myeloid stromal cells. *Br. J. Haematol.*, 98(2):274–282, 1997.

R. J. Shipley, A. J. Davidson, K. Chan, J. B. Chaudhuri, S. L. Waters, and M. J. Ellis. A strategy to determine operating parameters in tissue engineering hollow fiber bioreactors. *Biotechnol. Bioeng.*, 108(6):1450–1461, 2011.

T. Simsek, F. Kocabas, J. Zheng, R. J. DeBerardinis, A. I. Mahmoud, E. N. Olson, J. W. Schneider, C. C. Zhang, and H. A. Sadek. The distinct metabolic profile of hematopoietic stem cells reflects their location in a hypoxic niche. *Cell Stem Cell*, 7(3):380–390, 2010.

D. D. Van Slyke and J. M. Neill. The determination of gases in blood and other solutions by vacuum extraction and manometric measurement. i. *Journal of Biological Chemistry*, 61(2): 523–573, 1924.

H. R. Tahhan, C. T. Holbrook, L. R. Braddy, L. D. Brewer, and J. D. Christie. Antigen-matched donor blood in the transfusion management of patients with sickle cell disease. *Transfusion*, 34(7):562–569, 1994.

G. Terszowski, C. Waskow, P. Conradt, D. Lenze, J. Koenigsmann, D. Carstanjen, I. Horak, and H. R. Rodewald. Prospective isolation and global gene expression analysis of the erythrocyte colony-forming unit (CFU-E). *Blood*, 105(5):1937–1945, 2005.

N. E. Timmins and L. K. Nielsen. Blood cell manufacture: current methods and future challenges. *Trends in Biotechnology*, 27(7):415–422, 2009.

N. E. Timmins, S. Athanasas, M. Guenther, P. Buntine, and L. K. Nielsen. Ultra-high-yield manufacture of red blood cells from hematopoietic stem cells. *Tissue Eng. Part C-Methods*, 17(11):1131–1137, 2011.

E. Velliou, M. Fuentes-Garí, R. Misener, E. Pefani, M. Rende, N. Panoskaltsis, E. N. Pistikopoulos, and A. Mantalaris. A framework for the design, modeling and optimization of biomedical systems. In J. D. Siirola M. Eden and G. P. Towler, editors, *Proceedings of the 8th International Conference on Foundations of Computer-Aided Process Design FOCAPD*, Computer-Aided Chemical Engineering, 2014. Accepted.

M. Vlaski, X. Lafarge, J. Chevaleyre, P. Duchez, J.-M. Boiron, and Z. Ivanovic. Low oxygen concentration as a general physiologic regulator of erythropoiesis beyond the epo-related downstream tuning and a tool for the optimization of red blood cell production ex vivo. *Experimental Hematology*, 37(5):573 – 584, 2009.

W. Wang, D. N. Horner, W. L. K. Chen, P. W. Zandstra, and J. Audet. Synergy between erythropoietin and stem cell factor during erythropoiesis can be quantitatively described without co-signaling effects. *Biotechnol. Bioeng.*, 99(5):1261–1272, 2008.

B.I. Whitaker and R.A. Henry. The 2011 nationwide blood collection and utilization survey report, 2011. Department of Health and Human Services, U.S.A.

R. Willaert, A. Smets, and L. De Vuyst. Mass transfer limitations in diffusion-limited isotropic hollow fiber bioreactors. *Biotechnol. Tech.*, 13(5):317–323, 1999.

A. Wodnar-Filipowicz, S. Yancik, Y. Moser, V. D. Carbonare, A. Gratwohl, A. Tichelli, B. Speck, and C. Nissen. Levels of soluble stem-cell factor in serum of patients with aplastic-anemia. *Blood*, 81(12):3259–3264, 1993.

World Health Organization. Global database on blood safety, 2011. www.who.int/bloodsafety/global_database/GDBS_Summary_Report_2011.pdf; Accessed 09 Sept 2013.

H. Wu, X. Liu, R. Jaenisch, and H. F. Lodish. Generation of committed erythroid BFU-E and CFU-E progenitors does not require erythropoietin or the erythropoietin receptor. *Cell*, 83 (1):59–67, 1995.

D. Yeo, A. Kiparissides, J. M. Cha, C. Aguilar-Gallardo, J. M. Polak, E. Tsiridis, E. N. Pistikopoulos, and A. Mantalaris. Improving embryonic stem cell expansion through the combination of perfusion and bioprocess model design. *PLOS ONE*, 8(12), 2013.

S. H. Yoon, H. S. Kim, and I. T. Yeom. Optimization model of submerged hollow fiber membrane modules. *J. Membr. Sci.*, 234(1-2):147–156, 2004.

M. E. Young, P. A. Carroad, and R. L. Bell. Estimation of diffusion-coefficients of proteins. *Biotechnology Bioengineering*, 22(5):947–955, 1980.

H. Youssoufian, G. Longmore, D. Neumann, A. Yoshimura, and H. F. Lodish. Structure, function, and activation of the erythropoietin receptor. *Blood*, 81(9):2223–2236, 1993.

Appendix A. Optimisation Problem

$$
\begin{aligned}
\text{min} \quad & \left[\sum_{k \in \{\text{EPO; SCF}\}} p_k \cdot \tau_k \cdot N_{\text{R}} \cdot \text{Vol}_{\text{Recyc}} \cdot C_{k,\text{IN}} + p_k \cdot D \cdot V_k \cdot \text{Vol}_T \right] + \\
& \left[\sum_{h \in \{Q;\, E;\, G;\, L\}} p_{\text{UCB}} \cdot H_{h,0} \cdot \text{Vol}_T \right] \\
\text{s.t.} \quad & \\
\text{Superstructure Topology} \quad & \begin{cases}
N_{\text{HF}} = N_{\text{HF,PAN}} + N_{\text{HF,CRM}} \\
\varepsilon_{\text{R,HF}} \cdot R_4^2 \geq N_{\text{HF,PAN}}\, R_{2,\text{PAN}}^2 + N_{\text{HF,CRM}}\, R_{2,\text{CRM}}^2 \\
\text{Vol}_R = \pi\, (L - L_e) \left[R_4^2 - N_{\text{HF,PAN}}\, R_{2,\text{PAN}}^2 - N_{\text{HF,CRM}}\, R_{2,\text{CRM}}^2 \right] \\
\text{Vol}_{K,k} = \begin{cases} \frac{\pi \cdot (L - L_e) \cdot R_4^2}{N_{\text{HF,PAN}}} & k = \text{Glc, Lac} \\ \frac{\pi \cdot (L - L_e) \cdot R_4^2}{N_{\text{HF,CRM}} + N_{\text{HF,PAN}}} & k = \text{O}_2 \\ \frac{\pi \cdot (L - L_e) \cdot R_4^2}{N_{\text{HF,CRM}}} & k = \text{EPO, SCF} \end{cases} \\
R_{3,k} = \sqrt{\frac{\text{Vol}_{K,k}}{\pi\, (L - L_e)}} \quad \forall\, k \\
\text{Vol}_T = N_{\text{R}}\, \text{Vol}_{\text{R}}
\end{cases} \\
\text{Production Requirement} \quad & \begin{cases}
H_{Q,t} + H_{L,t} + H_{E,t} + H_{G,t} \leq H_{\text{MAX}} \\
\gamma_{P,t} = J_{\text{Cells},t} \cdot \pi \cdot N_{\text{HF,CRM}} \cdot R_{2,\text{CRM}} \cdot L \; \forall t \in \{1, \ldots, 5\} \\
\sum_t \gamma_{P,t}\, D_t\, H_{E,t} \geq \text{Unit}_{\text{RBC}}
\end{cases} \\
\text{Species Transfer} \quad & \begin{cases}
C_{k,\text{MIN}} \leq C_{k,i}(r,z) \leq C_{k,\text{MAX}} & \forall\, i, k \\
C_{k,\text{OUT}} = \left(R_2 - \frac{R_3^2}{R_2} \right) \cdot \left(\frac{\text{N}_{HF} \cdot \text{V}_k}{U_Z} \right) + \text{C}_{k,\text{IN}} & \forall\, k \\
C_{k,\text{LOSS}} = \frac{V_k}{D_{k,3}} \left(R_3^2 - R_2^2 \right) \left(\frac{11}{48} + \frac{1}{2 \cdot \varepsilon_{HF}} \ln \frac{R_2}{R_1} \right) & \forall\, k \\
C_{k,3}(R_2, 0) = C_{k,\text{IN}} - C_{k,\text{LOSS}} & \forall\, k \\
C_{k,3}(R_3, L) = \frac{V_k}{D_{k,3}} \left(\frac{R_3^2}{2} \ln \frac{R_3}{R_2} - \frac{R_3^2 - R_2^2}{4} \right) + C_{k,\text{OUT}} - C_{k,\text{LOSS}} & \forall\, k
\end{cases} \\
\text{Proliferation \& Differentiation} \quad & \begin{cases}
\frac{H_{Q,t} - H_{Q,t-1}}{\Delta t} = -\left(\kappa_{E,t-1} + \kappa_{G,t-1} + \kappa_{L,t-1} \right) \cdot H_{Q,t-1} \\
\qquad + (2 \cdot e^{-\gamma_S \cdot \tau_Q} - 1) \cdot \beta_{Q,t-1} \cdot H_{Q,t-1} \\
\frac{H_{E,t} - H_{E,t-1}}{\Delta t} = -(\gamma_E + \gamma_{P,t}) \cdot H_{E,t-1} + A_E \cdot \kappa_{E,t-1} \cdot H_{Q,t-1} \\
\frac{H_{L,t} - H_{L,t-1}}{\Delta t} = -(\gamma_L + \gamma_{P,t}) \cdot H_{L,t-1} + A_L \cdot \kappa_{L,t-1} \cdot H_{Q,t-1} \\
\frac{H_{G,t} - H_{G,t-1}}{\Delta t} = -(\gamma_G + \gamma_{P,t}) \cdot H_{G,t-1} + A_G \cdot \kappa_{G,t-1} \cdot H_{Q,t-1} \\
\qquad \forall\, t \in \{1, \ldots, 5\}
\end{cases}
\end{aligned}
$$

Appendix B. Data, Definitions and Parameter Values

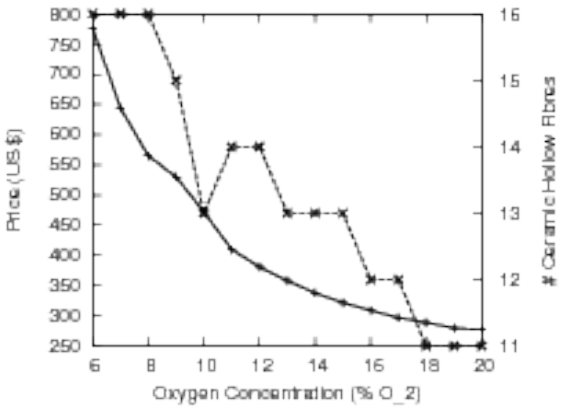

(a) Maximum environmental glucose level: 25 mM

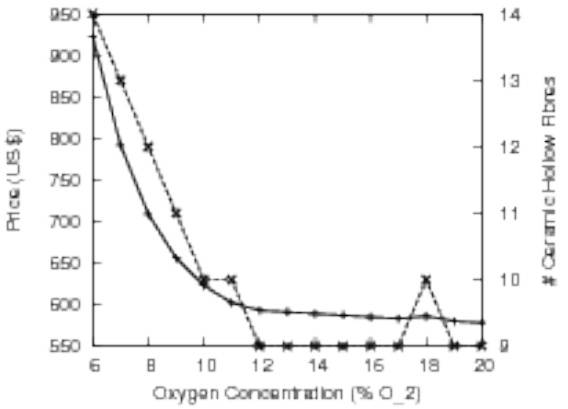

(b) Maximum environmental glucose level: 5.5 mM

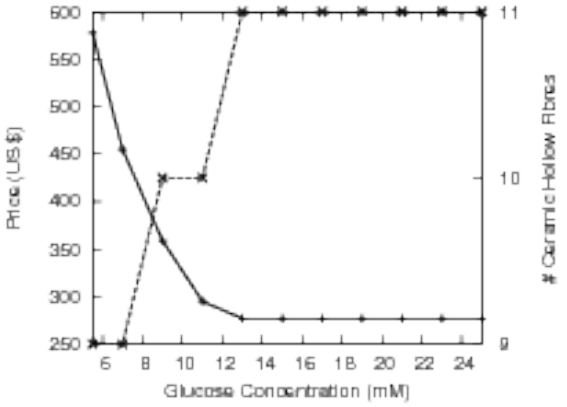

(c) Maximum environmental O_2 level: 20%

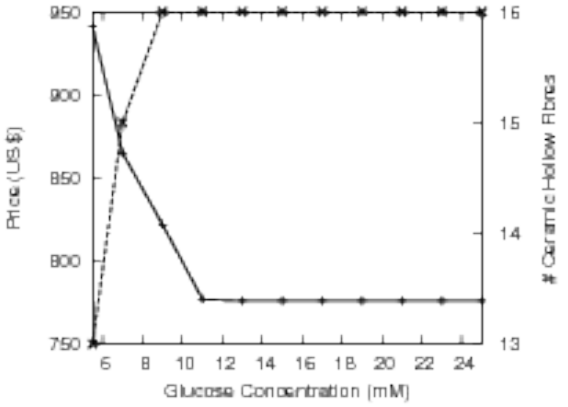

(d) Maximum environmental O_2 level: 6%

Figure 6: Bioreactor cost (solid line in each subfigure) and integer number of ceramic HF (dashed line in each subfigure) versus changing environmental conditions. Naturally, it is least expensive to provide very high levels of glucose (25 mM when maximum physiological BM levels are 5.5 mM) and O_2 (20% when maximum physiological BM levels are 6%). But artifically-high levels of nutrients and metabolites may introduce cell-altering artifacts into the *in vivo* culture, so it is interesting to see the changing configurations with the more restrictive environmental conditions.

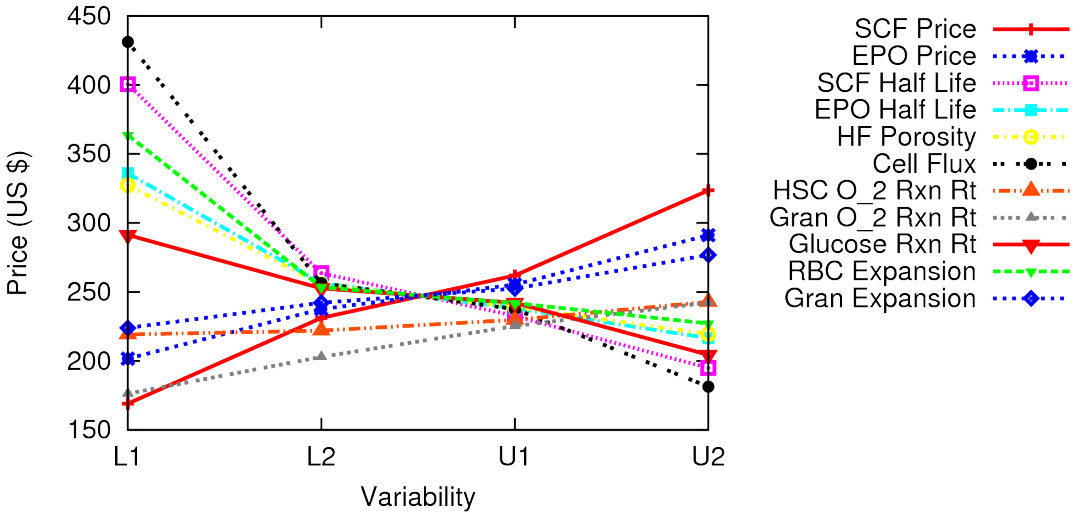

Figure 7: Parameter sensitivity analysis for the 11 parameters inducing the global optimum to change by 10% or more; all but reaction rates of O_2 with HSC and granulocytes were allowed to take values 50% (L1), 90% (L2), 110% (U1), and 150% (U2) of their nominal values. The range in O_2 reaction rates was taken from Table 7.

Table B.9: Definitions

	Symbol	Description	Units	Source
Abbrev-iations	BM	Bone marrow		
	HF	Hollow fibre		
	HFMB	Hollow fibre membrane bioreactor		
	HSC	Haematopoietic stem cell		
	PAN	Polyacrylonitrile		
	PU	Polyurethane		
	RBC	Erythrocyte; red blood cell		
	UCB	Umbilical cord blood		
Indices	h	Haematopoietic cells; $h \in \{Q, E, L, G\}$ where $Q \equiv$ HSC, $E \equiv$ RBC, $L \equiv$ lymphocytes, $G \equiv$ granulocytes		
	i	Bioreactor region; $i \in \{1, \ldots, I\}$ where $1 \equiv$ hollow fibre lumen, $2 \equiv$ hollow fibre membrane, $3 \equiv$ polyurethane scaffold; one Krogh cylinder, $4 \equiv$ entire bioreactor		
	k	Species; $k \in \{\text{Glc}, \text{Lac}, \text{O}_2, \text{EPO}, \text{SCF}\}$ where Glc $\equiv$ glucose, Lac $\equiv$ lactate, $\text{O}_2 \equiv$ oxygen, EPO $\equiv$ erythropoietin, SCF $\equiv$ stem cell factor		
	t	Time period in weeks; $t \in \{1, \ldots, 5\}$		
Parameters	$C_{k,\text{MIN}}$	Allowable concentration range of species k		Table 3
	$C_{k,\text{MAX}}$	$C_{\text{Glc}}, C_{\text{Lac}}, C_{\text{O2}}$ [=] $\frac{\text{mol}}{\text{m}^3}$; C_{EPO} [=] $\frac{\text{U}}{\text{m}^3}$; C_{SCF} [=] $\frac{\text{mg}}{\text{m}^3}$		
	D	Days at steady state culture conditions	35 days	Macedo (2011)
	$\varepsilon_{\text{R,HF}}$	Maximum HF packing density in reactor	0.14	Macedo (2011)
	H_{MAX}	Maximum cell density	0.5×10^{-6} cells / mm^3	
	R_i	Radius of region $i \in \{1, 2\}$	$R_{\text{CRM},1}$ = 0.25 mm; $R_{\text{CRM},2}$ = 0.43 mm	Macedo (2011)
			$R_{\text{PAN},1}$ = 0.26 mm; $R_{\text{PAN},2}$ = 0.45 mm	Macedo (2011)
	Unit_{RBC}	Number of RBC in one unit	2×10^{12} cells	Timmins and Nielsen (2009)
	$\text{Vol}_{\text{Recyc}}$	Recycle volume needed for each reactor	1.0×10^{-4} m^3	est.

continued on the next page

Table B.9 (Definitions) continued

	Symbol	Description	Units	Source
Uncertain Parameters	A_h	Amplification parameter for differentiation $h \in \{E, L, G\}$	$A_E = 5.63 \times 10^5$; $A_G = 2.82 \times 10^5$; $A_L = 7.52 \times 10^4$	Colijn and Mackey (2005)
	$D_{k,i}$	Diffusivity of species k in region $i \in \{1, 2, 3\}$	m^2/s	Table 4
	ε_{PU}; ε_{HF}	Porosity of HF and PU scaffold	$\varepsilon_{PU} = 0.79 \pm 0.1$; $\varepsilon_{HF} = 0.8$	Macedo (2011)
	γ_h	Death rate (non-age) of differentiated cells; $h \in \{E, L, G\}$	$\gamma_E = 0.001$ days^{-1}; $\gamma_G = 0.15$ days^{-1}; $\gamma_L = 2.4$ days^{-1}	Colijn and Mackey (2005)
	γ_Q	Death rate of HSC during proliferation	0.1 days^{-1}	Colijn and Mackey (2005)
	$\hat{J}_{Cells}$	Cellular flux across ceramic HF when $\Delta\hat{H}_{Cells} = 1.00 \times 10^6$ cells / mm^3	$\hat{J}_{Cells} = 5.76 \pm 2.25 \times 10^5$ cells / mm^2 / day	(Macedo, 2011, p. 177)
	p_k	Price of species k	$p_{EPO} = 0.023 \frac{US\ \$}{U}$; $p_{SCF} = 320 \frac{US\ \$}{mg}$	R&D Systems
	p_{UCB}	Price of umbilical cord blood	US \$ 220 / 4.0×10^8 nucleated cells	NHS (2013)
	$t_{1/2,k}$	Growth factor half-life	$t_{1/2,EPO} = 3$ days[2]; $t_{1/2,SCF} = 2$ days	Kishimoto et al. (2010)
	τ_Q	Stem Cell Proliferation time	1.4 days	Colijn and Mackey (2005)
	V_k	Maximum rxn rate of species k in the scaffold	$V_{Glc}, V_{Lac}, V_{O2}\,[=] \frac{mol}{m^3\ day}$; $V_{EPO}\,[=] \frac{U}{m^3\ day}$; $V_{SCF}\,[=] \frac{mg}{m^3\ day}$	Section 4.6
	$V_{O_2,h}$	Rxn rate of O_2 with cell type h in the scaffold	$V_{O_2,HSC} = 3.89 \times 10^{-14} \frac{mol}{cell\ day}$; $V_{O_2,RBC} = 1.56 \times 10^{-13} \frac{mol}{cell\ day}$ $V_{O_2,Gran} = 1.56 \times 10^{-11} \frac{mol}{cell\ day}$; $V_{O_2,Leuk} = 1.2 \times 10^{-12} \frac{mol}{cell\ day}$	Chow et al. (2001)
Decision Variables	$C_{k,IN}$	Conc. of species k at bioreactor inlet	$C_{Glc}, C_{Lac}, C_{O2}\,[=] \frac{mol}{m^3}$; $C_{EPO}\,[=] \frac{U}{m^3}$; $C_{SCF}\,[=] \frac{mg}{m^3}$	Table 3
	L	Length of Bioreactor	$\hat{L} = 150$ mm; $L \in [50$ mm, 200 mm$]$	Macedo (2011)[3]
	N_{HF}	Number of hollow fibres	$\hat{N}_{HF} = 8$; $N_{HF} \in \{1, \ldots, 20\}$	Macedo (2011)

continued on the next page

[2] An NHS pharmacist advised us that *the patient may ... store [EPO] at room temperature for up to three days*

[3] Variables marked with ˆ denote design choices of Macedo (2011)

Table B.9 (Definitions) continued

	Symbol	Description	Units	Source
Decision Variables	$N_{HF,CRM}$	Number of ceramic HF	$\hat{N}_{HF,CRM} = 4$; $N_{HF,CRM} \in \{1, \ldots, 20\}$	Macedo (2011)
	$N_{HF,PAN}$	Number of polymeric HF	$\hat{N}_{HF,PAN} = 4$; $N_{HF,PAN} \in \{1, \ldots, 20\}$	Macedo (2011)
	N_R	Number of equivalent bioreactors	$\hat{N}_R = 1$	Macedo (2011)
	R_4	Radius of region $i = 4$ mm	$\hat{R}_4 = 3.75$ mm; $R_4 \in [2, 10]$	Macedo (2011)
	U_Z	Bulk liquid velocity in the HF	$\hat{U_Z} = 7.1 \times 10^{-2} \frac{mm}{s}$; $U_Z \in [\hat{U_Z}, 2 \cdot \hat{U_Z}]$	Macedo (2011)
Dependent Variables	$\beta_{Q,t}$	Rate of entry into the proliferative phase	$days^{-1}$	Colijn and Mackey (2005)
	$C_{k,i}(r, z)$	Conc. of species k in region i at location (r, z)		Eqs. (20) – (22)
		$C_{Glc}, C_{Lac}, C_{O2}\,[=]\,\frac{mol}{m^3}$; $C_{EPO}\,[=]\,\frac{U}{m^3}$; $C_{SCF}\,[=]\,\frac{mg}{m^3}$		
	$C_{k,OUT}$	Conc. of species k at bioreactor outlet		Eq. (23)
		$C_{Glc}, C_{Lac}, C_{O2}\,[=]\,\frac{mol}{m^3}$; $C_{EPO}\,[=]\,\frac{U}{m^3}$; $C_{SCF}\,[=]\,\frac{mg}{m^3}$		
	$\gamma_{P,t}$	Production rate of cells from the bioreactor	$days^{-1}$	Eq. (47)
	$H_{h,t}$	Cell types $h \in \{Q, E, L, G\}$ in region 3 for $t \in \{1, \ldots, 5\}$	cells / m^3	Eqs. (38) – (41)
	J_{Cells}	Cellular flux across ceramic HF		Eq. (47)
	$\kappa_{h,t}$	Differentiation rate towards committed lineages $h \in \{E, L, G\}$	$days^{-1}$	Colijn and Mackey (2005)
	R_3	Radius of region $i \in \{3\}$	mm	Eq. (12)
	r	Radial distance from centre of Krogh cylinder	mm	
	Rxn_k	Reaction Rate of Species k		Eq. (18); 0^{th}-order approx
		$R_{Glc}, Rxn_{Lac}, Rxn_{O2}\,[=]\,\frac{mol}{m^3\ day}$; $Rxn_{EPO}\,[=]\,\frac{U}{m^3\ day}$; $Rxn_{SCF}\,[=]\,\frac{mg}{m^3\ day}$		
	τ_k	Rate for replenishing growth factor	–	Eq. (45)
	$Vol_{K,k}$	Krogh volume for each species $k \in \{Glc, Lac, O_2, EPO, SCF\}$	m^3	Eq. (11)
	Vol_R	Reactor volume	m^3	Eq. (10)
	Vol_T	Total volume	m^3	Eq. (13)
	z	Axial distance along the bioreactor	mm	

Table B.8: Raw Bioreactor Data

Day	Glc Conc. [mM] at HF exit				Lac Conc. [mM] at HF exit				pH at HF exit				O_2 [mm Hg] at HF exit			
	PAN		Ceramic		PAN		Ceramic		PAN		Ceramic		PAN		Ceramic	
	A	B	A	B	A	B	A	B	A	B	A	B	A	B	A	B
0																
1	23.8	22.0	20.1	20.0	0.0	0.0	5.8	3.2	7.53	7.56	7.53	7.61	204	192	203	234
3	23.1	23.0	19.4	21.2	2.7	0.0	6.9	2.7	7.51	7.55	7.48	7.59	182	189	208	207
5	22.9	22.4	18.6	21.8	3.6	2.8	9.4	3.4	7.48	7.52	7.37	7.52	187	179	207	238
7	21.1	22.4	16.2	21.1	7.4	4.7	14.6	5.1	7.37	7.44	7.21	7.50	177	172	230	213
9	19.2	23.1	14.1	20.0	11.7	2.7	20.3	7.0	7.41	7.63	7.04	7.47	196	179	192	219
11	18.3	19.2	13.2	19.2	14.7	9.0	21.4	9.4	7.24	7.35	6.97	7.44	161	170	200	210
13	17.5	18.7	18.7	21.8	14.7	10.0	21.6	11.8	7.21	7.34	6.96	7.33	191	195	213	222
15	17.7	18.1	18.7	21.3	14.9	11.0	21.3	14.2	7.26	7.43	7.00	7.28	197	194	212	222
22	19.0	21.1	20.1	21.9	13.4	10.0	20.0	17.1	7.22	7.38	7.02	7.13	183	186	206	213
24	18.8	21.0	20.0	21.6	13.8	10.0	19.9	17.0	7.33	7.45	7.04	7.18	191	191	213	186
26	20.6	22.4	20.1	22.2	11.1	6.3	20.3	17.0	7.35	7.47	7.03	7.12	190	188	188	200
28	19.3	22.2	19.9	20.7	11.6	6.1	20.0	17.4	7.31	7.46	7.01	7.12	170	177	179	194
31	19.2	21.7	21.2	22.2	14.8	9.3	19.6	15.9	7.19	7.35	7.07	7.16	142	143	171	174
Ave[†]	19.1	21.0	18.2	21.2	12.8	7.9	19.9	13.2	7.29	7.43	7.04	7.27	180	180	200	205
	19.9				13.5				7.26				191			
Std Dev[†]	1.1	1.7	2.8	1.0	2.4	2.8	2.0	4.6	0.08	0.09	0.07	0.15	18	16	18	16
	2.1				5.2				0.17				19			

[†] Averages and standard deviations equally weight data from days 7 – 31; the start-up lag phase is ignored